



NTNU – Trondheim
Norwegian University of
Science and Technology

Laser light deformation of microdroplets

Petter Tømmerås Bossum

Master of Science in Physics and Mathematics

Submission date: December 2014

Supervisor: Morten Kildemo, IFY

Co-supervisor: Simen Andreas Ådnøy Ellingsen, EPT

Norwegian University of Science and Technology
Department of Physics

Abstract

This masters work describes the deformation of a droplet that is illuminated by a laser beam. The theory for linear fluid mechanical motion of the droplet is discussed. This is combined with Lorenz-Mie scattering. Droplet deformations resulting from the optical radiation pressure are computed.

Specific beam profiles are discussed in the literature for the purposes of optical droplet deformation, namely the cases of linear and circular polarized plane waves, a Gaussian beam and the Bessel beam. The general case of an arbitrary beam is not, to the author's knowledge, given in the published literature. Such a framework is developed from first principles and presented in this work.

A Mathematica script was written to compute deformations. These are calculated, fitting nicely to those found by Ellingsen in a recent article. The case of two plane waves from opposite directions is discussed here for the first time, and droplet shapes produced.

The size droplets considered is between the geometrical limit and the Rayleigh limit. The numerical load increases quickly with increasing values of the droplet radius and wave vector. The hardest to compute coefficients die off the most quickly with time.

Abstract

I denne masteroppgaven beskrives deformasjonen til en liten dråpe som treffes av en laser-stråle. Lineær fluidmekanikk og Lorens-Mie-teori blir kombinert for å beskrive dette systemet. Dråpeformer er funnet med numeriske beregninger.

Tidligere arbeid for å beskrive dråpe-deformasjoner under laserlys beskriver et knippe spesifikke laserprofiler. Det generelle tilfellet med en vilkårlig laserprofil er, så langt forfatteren vet, ikke beskrevet i den utgitte litteraturen på feltet. Et teoretisk rammeverk for å beskrive dette tilfelle utvikles og beskrives i dette arbeidet.

Et program er skrevet i Mathematica, for å kalkulere dråpeformer for de ulike laserprofilene. Tilfellet med en enkelt laser-stråle fra venstre, med planbølge eller gaussisk profil, er utforsket. Svarene passer med tidligere publiserte resultater. Tilfellet med to planbølger er beskrevet for første gang her, og dråpeformer gitt.

Størrelsen på dråpene som er sett på ligger mellom geometrisk optikk og Rayleigh-grensen. Det numeriske arbeidet blir tyngre for større dråper, men de leddene det er vanskeligst å beregne er de som forsvinner først når dråpen oscillerer.

Contents

1	Introduction	4
2	Theory	7
2.1	Assumptions of the system.	7
2.1.1	Spherical droplet	7
2.1.2	Electrostriction	8
2.2	Fluid Mechanics	9
2.2.1	Identifying the terms in Navier-Stokes.	9
2.2.2	Choosing an expansion and normalizing it.	10
2.2.3	Expanding the fluid mechanics into associated Legendre polynomials	11
2.2.4	Combining the terms, and solving for h	13
2.3	Electromagnetics	13
2.3.1	Maxwells stress tensor	13
2.3.2	Expanding the fields.	14
2.3.3	Refraction and surface force density.	16
2.3.4	Power and Intensity	17
2.4	Organizing for numerical work.	18
2.4.1	Rewriting the surface force density.	18
2.4.2	Expansion of the formalism: use of associated Legendre Polynomials.	19
2.4.3	Computational complexity	21
2.5	Different cases for the incoming fields	22
2.5.1	Single plane wave, or Gaussian beam, with circular polarization.	22
2.5.2	Plane waves from opposite sides of the droplet.	25
3	Numerical calculations	28
3.1	Plane wave and Gaussian wave from one side.	28
3.2	Plane wave beams from both sides.	29
4	Discussion and conclusion	31
5	Appendix A, Mathematica scripts.	33

1 Introduction

The field of optofluidics is the combination of microfluidics and optics; controlling liquids with light and using liquids as optical elements.

A tightly focused laser beam can trap particles and bubbles. The light interacts with a dielectric particle, exerting forces on it. With a suitable laser profile this becomes a potential well, keeping the particle or bubble in place. These optical tweezers allow detailed manipulation of microsystems, well suitable for a range of biological applications, where optical tweezers already see use [1]. Grier et.al. [1] also outline a wide range of possible uses from motors in microengineering to measurements of molecular interaction.

Optical sorting of particles was demonstrated by MacDonald et.al. [2]. The diffraction pattern of a split beam produced an optical lattice capable of sorting particles efficiently, based on size or refractive index. See also Guck et.al. [3] that stretched a dielectric cell using two optical traps opposite to each other. Their specimen was a red blood cell, used for its softness, producing shapes similar to the ones with the case of a droplet. Another interesting example of droplet manipulation work is done by Ward et.al., aptly named "optical sculpting". A number of traps sculpt droplet of very low surface tension into various shapes [4], see Figure 1.

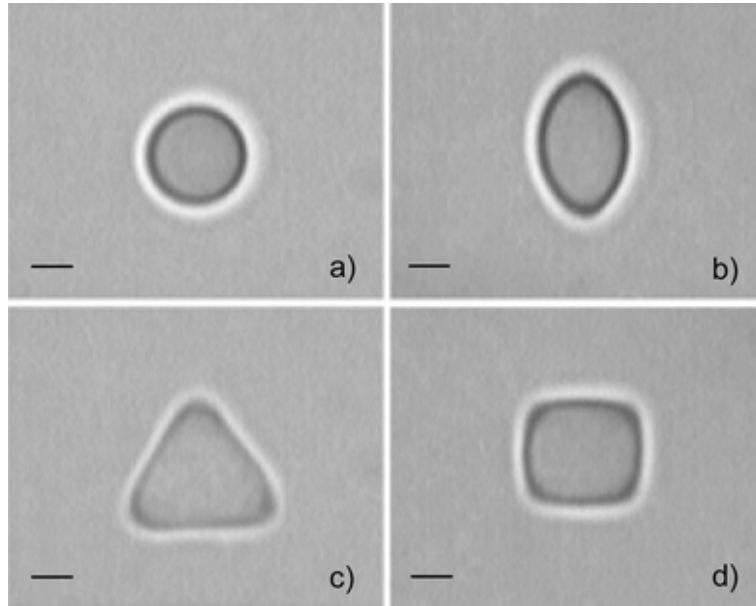


Figure 1: Emulsion droplets, with low surface tension, deformed by a number of traps, from Ward et.al. [4]. One trap in a), two in b), three in c) and four in d), as can be guessed from the resulting deformations.

As well as trapping particles, a laser beam can push them. This case is easily imagined, thinking in terms of radiation pressure. However, Chen et.al. [5] recently showed how a beam can pull a droplet towards it, opposite to the travelling direction of the wave. Following the images in [6], the effect is easier to grasp in Fourier optics. Consider the beam as an ensemble of sine waves. These individual waves do not travel

in the same direction, but together they form a beam. When the droplet scatters the light to collimate these, there is a net momentum backwards, and thus a tractor beam!

Development in micromanufacture has led to recent development of, and interest for, lab-on-chip systems, see e.g. [7] for a review. The essence is that fluids can be transported and manipulated on chips, with microfluidic channels. This could automate laboratory work, especially in chemistry and biology, as is alluded to in the name. A crucial element in these chips is the integration of lasers for the handling of the liquids. See Psaltis and Li [8] for a discussion of the different laser methods used.

Droplets can prove to be useful in these chips, as described by Baroud et.al. [9]. They can be moved, manipulated, split and even deformed into a desired shape, using electrostatics, acoustics or laser optics. Droplets can be used as microreactors, e.g. in [10], containing the materials undergoing a reaction. The future seems promising for the use of droplets in these systems.

A classical experiment on droplets was performed by Chang and Zhang in 1989 [11], where a droplet was photographed as a laser beam hit it. See figure 2 for these droplet photographs. The results were soon explained [12] using the Mie solutions for the electrodynamic fields. These articles typically call the force in question "electrostriction". This is something of a misnomer, as shall be seen later. Brevik and Kluge [13] found the oscillations for a pulse of linearly polarized light. Ellingsen recently found the motion for a Gaussian beam [14], and the case where the droplet is pulled in the opposite direction of the beam [15].

My advisor, Simen. Å. Ellingsen, and colleagues, are planning experimental work with the Central Laser Facility in the UK. To make sure that the droplet does not gain momentum, and fly away, it is exposed to two identical beams from opposite sides. Calculating how the droplet will react to two pulses will therefore be a necessary requisite.

The procedure follows the one found in the previous work, e.g. [12–14]

1. The electromagnetic surface force density is calculated for a spherical droplet at rest.
2. The surface perturbations are calculated with the linearized Navier-Stokes' equation, using the EM force.
3. The perturbations are assumed to be much smaller than the radius of the sphere. Thus a linear surface wave theory can be applied.

The equations involved are expanded in the spherical harmonics, or similarly with Legendre polynomials. This leaves an equation with a large amount of terms in the usual spherical harmonic parameters l, m with Y_l^m . Different systems allows for some, or most, of these terms to be ignored. The published work does this simplification early on in the calculation. This allows for easier calculation and less verbose texts.

The case of two plane waves from opposite sides of the droplet allows less terms to be ignored. This difference can be subtle, it simply includes higher orders of m for the surface force coefficients. Yet without a general expression of the equations involved, one has to go through

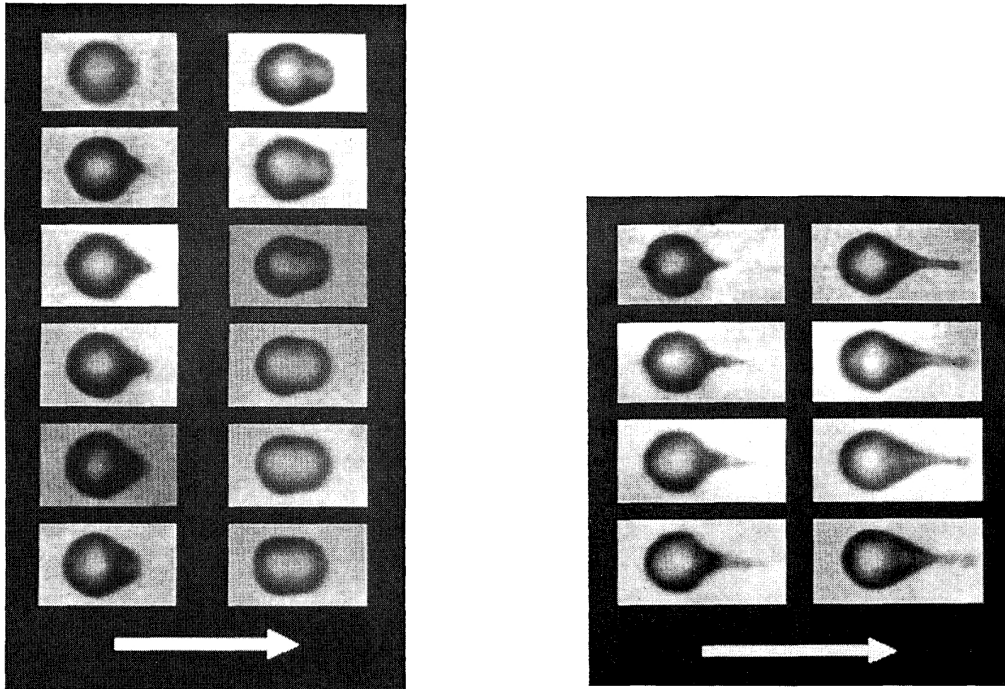


Figure 2: Photographs of laser irradiated water droplets, by Zhang and Chang [11]. Droplets are $100\mu\text{m}$ in diameter, time intervals of $2\mu\text{sec}$. Left: Pulse energy of 100mJ . Right: Pulse energy of 200mJ .

the entire framework to include the terms and check any relevant constants.

This treatment makes no assumptions about which terms to ignore. It is therefore expanded as if it had non-zero coefficients for all spherical harmonic functions. This gives a framework that will work with all available beams, including the case where beams come in from both sides. When a special case is investigated, the appropriate terms can be neglected, as before.

Numerical calculations are done for a droplet $4\mu\text{m}$ across. The shapes found in [14] are reproduced for the single incoming beam, with two systems. One is a water-droplet in air, as in Figure 2 (but with a smaller droplet). The other is the oil emulsion system used by Ward et.al., as in Figure 1.

The case of opposite plane wave beams is also investigated. Plausible droplet shapes are produced for the oil emulsion system. The script has issues when other systems are applied, such as the water in air system, or droplets significantly smaller. This gives strange results that is far more reasonable to denote to programming error, than actual results. Interestingly, the same general shape of the droplet is observed.

Much time has gone into bug-hunting in the code, with little result. Complete rewrites have been attempted, to no effect. Rewriting in a programming language better known to the author, or getting more familiar with Mathematica, would be a logical next step. The expansions contain terms that oscillate quickly, especially the terms not previously

considered. A problem with the stability of the integrals could explain some of the trouble nicely.

2 Theory

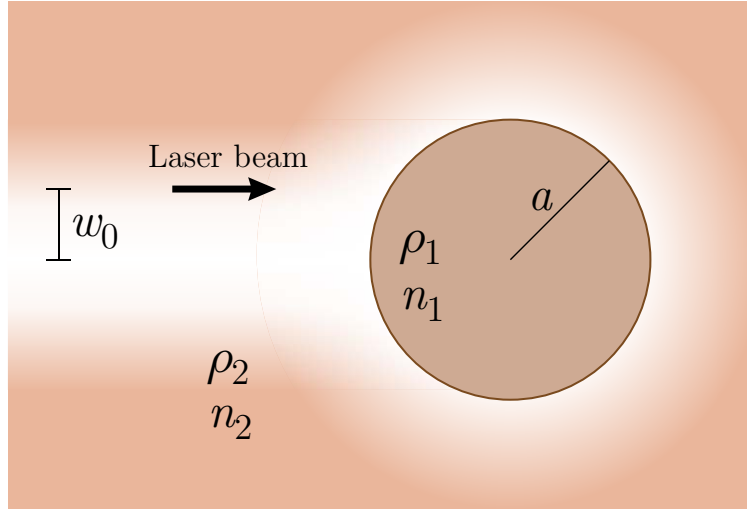


Figure 3: System considered, Figure obtained from Ellingsen [14]. A sphere of fluid 1, within fluid 2 is illuminated by laser beam. The beam waist is given, for the Gaussian case. In the plane wave limit, this waist is assumed infinite.

The system under consideration is shown in figure 3. A laser beam pushes the droplet, causing it to deform and oscillate. In the case of a pulse it returns to a sphere. For continuous operation it assumes a new equilibrium, allowing the surface tension to negate the force from the laser.

The exact profile of the incoming beam will be varied between a single plane wave, a single Gaussian wave and plane waves from opposite sides; all with circular polarization.

This chapter starts with a description of some assumptions of the system. Then the fluid mechanics and the electromagnetics are handled separately. The electrodynamics will produce an expression for the surface force density, which is applied in the fluid mechanics. The equations are massaged to a more concise and usable form, splitting them into a system-dependent part and constants that can be calculated once. This framework is then applied to the considered profiles of the incoming beams.

2.1 Assumptions of the system.

2.1.1 Spherical droplet

The droplet is assumed to remain spherical for the duration of the pulse. This enables the use of Generalized Lorenz-Mie Theory (GLMT). GLMT finds a solution to Maxwell's equations that is expressed in terms of the spherical harmonics, which are suitable for evaluation over the sphere.

With the fields in this form, the scattered fields can be found by applying the electrodynamic boundary conditions over the sphere. This results in an expression of the electromagnetic fields in the form of a spherical harmonic expansion.

If the droplet is deformed while subjected to the laser beam, it will diffract the light differently. This changes the forces, which again changes its shape and so on. Boyde et.al. recently found that surface stresses on a sphere versus a spheroid with an aspect ratio of 1.2 "hardly differed" [16], which supports the decision to ignore these effects for now.

In some cases the droplet deformation leads to a near spherical surface of the droplet, in the direction of the laser beam. The most important diffraction of the beam happens at this boundary. Using the curvature of the deformed sphere, one could approximate a new deformation, and so on. This way of approximation could be an interesting undertaking for the future.

The deformations are also assumed to be small in the fluid mechanical calculations, i.e. the calculations are done in the linear regime. This also limits the theoretic framework to beams with an intensity low enough to not excite too large deformations. Usefulness at the limits can be expected, as with general linear fluid mechanical theory [14].

2.1.2 Electrostriction

With the system considered, the electrodynamic forces consists of two terms [13]. These are the Abraham-Minkowski force (AB) and the electrostrictive force (ES). The AB-force acts on the boundary of the droplet, while the ES-force acts on the whole droplet, pushing towards the areas of higher electric or magnetic field intensity. Elastic pressure will build to cancel the ES-force, cancelling it, if there is enough time available.

Pressure builds up with the speed of sound in the medium. Over a droplet with radius a , the pressure thus builds up in a time [17]

$$\tau_c = \frac{2a}{u} \quad (1)$$

where u is the speed of sound in the medium. For pulses longer than this the elastic pressure will have time to counter any body forces, and the droplet can be considered incompressible, negating the ES-force.

For the cases observed in experiment and considered in the theory, this time is long enough compared to the pulse in question [17]. For example, droplets of water in air, used by Zhang and Chand [11], where $a = 50\mu m$ and $n = 1500m/s$, give a minimum laser pulse time of $\tau \leq 70ns$, well below the pulses used ($400 ns$). The droplets considered here are considerably smaller ($1-5 \mu m$), so the ES-force is assumed to be negligible.

Another note on electrostriction is the confusing use of language found in ref.s [11, 12]. The total electrodynamic forces on the droplet are called electrostrictive. The terminology used over is, as far as the author knows, the current way to look at it [17, 18]. This makes the older nomenclature a bit imprecise to look at, as the electrostrictive force is, indeed, negligible.

2.2 Fluid Mechanics

The droplet reaction to incoming light, in the linear regime, is explored. The approach used is the one found in references [12–15]. Navier-Stokes' equation is expanded in spherical harmonics. The equation is then solved termwise. The result is similarly found, using the velocity potential, in reference [19].

2.2.1 Identifying the terms in Navier-Stokes.

Take the linearised Navier-Stokes' equation, inside the droplet. The electrostrictive body force will, as discussed, be cancelled by a change in pressure. Following Brevik [13], we ignore these cancelling terms. This leaves

$$\frac{\partial \mathbf{v}}{\partial t} = -\frac{1}{\rho} \nabla p + \mu \nabla^2 \mathbf{v} \quad (2)$$

where p is the pressure, ρ is the fluid density, μ is the dynamic viscosity and \mathbf{v} is the fluid velocity. Note that the pressure p omits the cancelling ES-terms, akin to p^{AM} in [13]. We know that the electromagnetic forces affecting the droplet are all transverse to the spherical surface, or

$$\mathbf{f} = \sigma(\theta, t) \delta(r - a) \hat{\mathbf{r}} \quad (3)$$

in spherical coordinates (r, φ, θ) , where δ is the Dirac delta function. The motion to be calculated is therefore the radial motion of the droplet surface. We then choose to evaluate equation (2) at the droplet surface, just inside the droplet. The beam is assumed to be turned on at $t = 0$ and off at $t = t_0$. This allows the EM-force to be written as

$$\sigma(\theta, t) = \sigma(\theta) [\Theta(t) - \Theta(t - t_0)] \quad (4)$$

where $\Theta(t)$ is the Heaviside step function. This includes the static case in the special case where t_0 is set to infinity. This time-dependence is, a simpler version of the one found in [13], that takes the rise and fall time of the beam into account. These times are typically on the order of tens of nanoseconds [18].

The droplet surface is handily split into two parts

$$r(\theta, \varphi) = a + h(\theta, \varphi) \quad (5)$$

where a is the droplet radius and h is the displacement from a perfect sphere. The fluid velocity can then be written as:

$$\mathbf{v} = \dot{h}(\theta, \varphi) \hat{\mathbf{r}}, \quad \frac{\partial \mathbf{v}}{\partial t} = \ddot{h}(\theta, \varphi) \hat{\mathbf{r}} \quad (6)$$

At the surface, there will be two contributions to the pressure. The electromagnetic force will pull the surface, depending on the incoming fields and the refraction. The surface tension will pull the droplet surface back to the spherical shape. Thus

$$p = \Delta p^{\text{s.t.}} - \sigma(\theta, t) \quad (7)$$

where $\Delta p^{\text{s.t.}}$ denotes the surface tension contribution.

Both contributions to the pressure are only dependent on r , which gives

$$\Delta p = \frac{\partial p}{\partial r} \bar{\mathbf{r}} \quad (8)$$

for the pressure term.

This leaves an equation of motion

$$\dot{h}(\theta, \varphi) = -\frac{1}{\rho} \frac{\partial}{\partial r} (\Delta p^{\text{s.t.}} - \sigma(\theta, t)) + \mu \nabla^2 \mathbf{v} \quad (9)$$

for the system.

2.2.2 Choosing an expansion and normalizing it.

The spherical harmonics are usually normalized as

$$Y_{l,m}(\theta, \varphi) = \sqrt{\frac{2l+1}{4\pi} \frac{(l-m)!}{(l+m)!}} P_l^m(\cos \theta) e^{im\varphi} \quad (10)$$

with the associated Legendre Polynomials P_l^m . These are Orthonormal. In the previous work, one has not applied this normalization, but rather used $P_l^m(\cos \theta) e^{im\varphi}$ directly, taking care of the normalization in the expression for the expansion parameters. This is done here as well, both to keep close to previous work, and to avoid introducing dependencies in l, m in the fluid mechanical equations.

Take an arbitrary function

$$g(\Omega) = \sum_{l=1}^{\infty} \sum_{m=-l}^l g_{l,m} P_l^m(\cos \theta) e^{-im\varphi} \quad (11)$$

and invert it

$$g_{l,m} = \int g(\Omega) P_l^{m'}(\cos \theta) e^{-im'\varphi} d\Omega \quad (12)$$

$$= \sum_{l',m'} \int_0^{2\pi} e^{i\varphi(m-m')} d\varphi \int_{-1}^1 P_{l'}^{m'} P_l^m du \quad (13)$$

$$= 2\pi \frac{2}{2l+1} \frac{(l+m)!}{(l-m)!} \delta_{l,l'} \delta_{m,m'} \quad (14)$$

where the orthogonality of the Legendre Polynomials [20] is used. This should return be 1, which gives expansion parameters of

$$g_{l,m} = \frac{2l+1}{4\pi} \frac{(l-m)!}{(l+m)!} \int d\Omega g(\Omega) P_l^m(\cos \theta) e^{-im\varphi} \quad (15)$$

fitting nicely with the definition of the spherical harmonics.

Note that the expansion coefficients for σ will not carry much information about which parts contribute to the droplet form. This is a result of expanding σ on a basis that is orthogonal, but not normal. The choice made does conform closely to similar discussions in the literature consulted, and leads to a relatively easy to compute equation. Thus there is a trade-off here.

2.2.3 Expanding the fluid mechanics into associated Legendre polynomials

The next step is to expand every term of equation (9) in these Legendre polynomials. We define h and σ , and know little of them yet. They can easily be expanded to

$$h(t) = \sum_{l=1}^{\infty} \sum_{m=-l}^l h_{l,m} P_l^m \quad (16)$$

and

$$\sigma(\theta) = \sum_{l=1}^{\infty} \sum_{m=-l}^l \sigma_{l,m} P_l^m e^{im\varphi} \quad (17)$$

where the coefficients of σ are found to be

$$\sigma_{l,m} = \frac{(2l+1)(l-m)!}{4\pi(l+m)!} \int d\Omega \sigma(\Omega) P_l^m e^{-im\varphi} \quad (18)$$

whereas the expansion coefficients for h are the unknown found by this treatment. The coefficients for σ constitute the main numerical work, and will be found in the electrodynamics chapter.

Expanding the pressure is a bit more involved, as the radial part is involved as well. Following the derivation in [19], we start with the fact that $\nabla^2 p = 0$ [15], due to incompressibility and linear theory. This is written out as

$$\left(\frac{1}{r^2 \sin^2 \theta} \partial_\phi^2 + \frac{1}{r^2} \partial_r r^2 \partial_r + \frac{1}{r^2 \sin \theta} \partial_\theta \sin \theta \partial_\theta \right) p(r, \varphi, \theta) = 0 \quad (19)$$

in spherical coordinates. Assume we can separate the variables in p

$$p = T(t)R(r)\Theta(\theta)e^{im\varphi} \quad (20)$$

where the φ -dependence is expressed as a Fourier series. Inserting into equation (19) gives

$$\frac{\cos \theta \Theta'}{\sin \theta \Theta} + \frac{\Theta''}{\Theta} - \frac{m^2}{\sin^2 \theta} = -\frac{2rR' + r^2R''}{R} = -\mu^2 \quad (21)$$

arguing that since the radial and azimuthal parts are independent, and their sum zero, they must be equal. Substituting

$$u = \cos(\theta) \quad (22)$$

will be practical. This will change the derivatives in θ so that

$$\Theta'(\theta) = -\sin \theta \tilde{\Theta}'(u), \quad \Theta''(\theta) = -\cos \theta \tilde{\Theta}'(u) + \sin^2 \theta \tilde{\Theta}''(u) \quad (23)$$

when changing the variables in $\Theta(\theta)$ to $\tilde{\Theta}(u)$. Inserting this into equation(21) gives the familiar equation

$$(1-u^2)\tilde{\Theta}''(u) - 2u\tilde{\Theta}'(u) + \tilde{\Theta}(u)\left(\mu^2 - \frac{m^2}{1-u^2}\right) = 0 \quad (24)$$

that is recognized as the general Legendre differential equation. The solution is the associated Legendre polynomials $P_l^m(u), Q_l^m(u)$, introducing the integers l

$$\mu^2 = l(l+1) \quad (25)$$

and m . The terms are non-zero for

$$m \leq l \quad (26)$$

The pressure must be finite everywhere, the $Q_l^m(u)$ are not finite at $\theta = 0, \pi$, and are thus discarded. Using the new value of μ^2 we get

$$r^2 R'' + 2rR' - l(l+1)R = 0 \quad (27)$$

with solutions

$$R = \left(\frac{r}{a}\right)^l, \quad R = \left(\frac{r}{a}\right)^{1-l} \quad (28)$$

for R . The pressure inside the sphere, containing the origin, must be finite. The latter solution must therefore be discarded inside the sphere. Gathering the terms give

$$p(\theta, \varphi) = \sum_{l=1}^{\infty} \sum_{m=-l}^l \left(\frac{r}{a}\right)^l p_{l,m} P_l^m(\cos \theta) e^{im\varphi} \quad (29)$$

as the expanded pressure.

Calculating $\frac{\partial}{\partial r} p$ in with equation (29) gives

$$\frac{\partial}{\partial r} p = \frac{l}{a} p_{l,m} \quad (30)$$

in the boundary where $r \approx a$.

The viscous damping term is derived in [13]. The total energy of the system is considered, as in a harmonic oscillator, giving a damping term

$$\nu \Delta^2 v_r = -2 \sum_{l=1}^{\infty} \sum_{m=-l}^l \mu_{l,m} \dot{h}_l P_l(\cos \theta) e^{im\varphi} \quad (31)$$

$$\mu_{l,m} = \frac{\nu}{a^2} (2l^2 - l - 1) \quad (32)$$

where μ_l determines the life times of the various modes. In cases where $m \neq 0$ this becomes [13]

$$\mu_{lm} = \mu_l \quad (33)$$

such that μ_l is the same for all associated values of m .

The surface tension term can be written as [21]

$$\Delta p^{\text{s.t.}} = \gamma \left(\frac{1}{R_1} + \frac{1}{R_2} \right) \quad (34)$$

where R_1, R_2 are the principal radii of curvature of the surface. With expanded radius $r = a + h_l$ this becomes [21] [13]

$$\Delta p^{\text{s.t.}} = \frac{\gamma}{a^2} \sum_{l=1}^{\infty} \sum_{m=-l}^{m=l} (l^2 + l - 2) h_{l,m}(t) P_l(\cos \theta) \quad (35)$$

by assuming $h \ll a$ and discarding the $l = 0$ -terms.

2.2.4 Combining the terms, and solving for h .

Combining the terms in equation (2) at the boundary gives the termwise equation

$$\ddot{h}_{l,m} + 2\mu_{l,m}\dot{h}_{l,m} + \omega_l^2 h_{l,m} = \frac{l}{\rho a} \sigma_{l,m} [\Theta(t) - \Theta(t - t_0)] \quad (36)$$

$$\omega_l^2 = \frac{\gamma_l^l}{\rho a^3} (l^2 + l - 2) \quad (37)$$

where we have introduced ω_l . Applying the Laplace transform gives

$$\mathcal{L}\{h_{l,m}(t)\}(s) = \frac{l\sigma_{l,m}}{\rho a} \frac{1 - e^{-t_0 s}}{s(s^2 + 2\mu_l s + \omega^2)} \quad (38)$$

so that $h_{l,m}$ can be found by taking the inverse transform. This yields a result, as can be expected from a damped oscillator:

$$h_{l,m}(t) = h_{l,m}(\infty) \left[1 - \left(\frac{\mu_l}{\gamma_l} \sin \gamma_l t + \cos \gamma_l t \right) e^{-\mu_l t} \right] \Theta(t) - \left[1 - \left(\frac{\mu_l}{\gamma_l} \sin \gamma_l (t - t_0) + \cos \gamma_l (t - t_0) \right) e^{-\mu_l (t - t_0)} \right] \Theta(t - t_0) \quad (39)$$

$$h_{l,m}(\infty) = \frac{\sigma_{l,m} a^2}{\gamma_l} \frac{1}{l^2 + l - 2} \quad (40)$$

$$\gamma_l = \sqrt{w_l^2 - \mu_l^2} \quad (41)$$

$$\mu_l^2 = \frac{\gamma_l^l}{\rho_2 - \rho_1 a^3} (l^2 + l - 2) \quad (42)$$

where γ_l is the vibrational frequency, and μ_l the damping constant. Notice the lack of dependence upon m in these equations. This leads to them being easily compared to the similar results found in the reference material [14, 15]. The same shape is observed.

With a positive γ_l^2 the motion is underdamped, while a negative γ_l^2 , i.e. complex γ_l , gives an overdamped motion, replacing the sine terms with sinh terms and cos with cosh. The regions of underdamped vs. overdamped motion are worked out by Ellingsen [14], resulting in some quite large equations. For the droplet sizes discussed here, of a few μm , it can be summarized as follows: water droplets in air - underdamped, oil emulsions - underdamped, water bubbles in air - either.

For the static case, with infinite t_0 , the last term disappears, leaving the shape determined by $h_l(\infty)$ after a long time; hence the name. This will, as discussed earlier, be an approximation, as the new shape will diffract the light differently.

2.3 Electromagnetics

2.3.1 Maxwells stress tensor

The force density can be found by integrating the gradient of Maxwells stress tensor

$$\mathbf{T} = \mathbf{E} \otimes \mathbf{D} + \mathbf{H} \otimes \mathbf{B} - \frac{1}{2} (\mathbf{E} \cdot \mathbf{D} + \mathbf{H} \cdot \mathbf{B}) \mathbf{1} \quad (43)$$

over the surface of the droplet; here $\mathbf{1}$ denotes the identity matrix and $\mathbf{E}, \mathbf{D}, \mathbf{H}, \mathbf{B}$ are the complex fields for the incoming wave. These have time dependence

$$\mathbf{E} = \text{Re}\{(E_r + E_\theta + E_\varphi)e^{i\omega t}\} \quad (44)$$

where E_r, E_θ, E_φ are the complex field amplitudes in the corresponding directions. This gives

$$\langle E_r E_r \rangle = \frac{1}{2} |E_r|^2 \quad (45)$$

when taking the average over the optical period.

We assume the magnetic permeability to be equal to unity in both media, so that the magnetic fields are constant over the droplet boundary. They disappear from equation 43, resulting in

$$\mathbf{T}_{rr} = \frac{\epsilon_0 n^2}{2} (E_r^2 - E_\theta^2 - E_\varphi^2) \quad (46)$$

for the outward force on the bubble; ϵ_0 denotes the vacuum permittivity. The electromagnetic force on the boundary are then found to be

$$\sigma(\Omega) = \langle \sigma_{rr} \rangle = \langle T_{rr}(r = a^+) - T_{rr}(r = a^-) \rangle \quad (47)$$

where $\langle \dots \rangle$ denotes the mean over one optical period. Boundary conditions for the electric fields are given, e.g. in Jackson [20], as

$$n_1^2 \mathbf{E}_{\perp 1} = n_2^2 \mathbf{E}_{\perp 2}, \quad \mathbf{E}_{\parallel 1} = \mathbf{E}_{\parallel 2} \quad (48)$$

over the boundary between mediums 1, 2 as given in Figure 3. With the droplet geometry the perpendicular \perp direction is the r -direction, the other two being parallel \parallel . Combining equations (46,47,48) gives

$$\sigma(\Omega) = \frac{\epsilon_0 n_2^2}{4} (\bar{n}^2 - 1)(\bar{n}^2 |E_r^w|^2 + |E_\varphi^w|^2 + |E_\theta^w|^2) \quad (49)$$

where \mathbf{E}^w is the scattered field directly inside the droplet surface, at $r = a$. This simplifies the calculations as the fields outside the droplet need not be considered.

2.3.2 Expanding the fields.

Lorentz-Mie theory will now be applied to the incoming electric fields. The incoming fields are expressed in terms of spherical harmonics. The electromagnetic boundary conditions over a sphere are then applied. The resulting field can be described by three terms, The field inside the sphere, the incoming field and the scattered field. The fluid motion can, as discussed, be fully described by the internal field.

The task at hand then becomes to expand the incoming fields in spherical harmonics, and apply the appropriate boundary condition parameters. The results used are included as an appendix by Barton et.al. [22], widely used in the considered literature [12–15]. Derivations can also be found in [20] and [23], with different formalism.

Consider the fields (\mathbf{E} and \mathbf{H}) of an electromagnetic wave in a source free medium. The electric field can be expressed as a sum of two fields

$$\mathbf{E} = \mathbf{E}^{\text{TE}} + \mathbf{E}^{\text{TM}} \quad (50)$$

where the where TE and TM describe two directions. Transverse Electric (TE) fields are the fields that are perpendicular to the r-direction. The Transverse Magnetic fields are the fields that are not perpendicular to the r-direction. From Maxwells Equations we know that the electric and magnetic fields are perpendicular, thus the electric TM fields are the ones corresponding to a magnetic field that is perpendicular to the r-direction. From this one naturally have that

$$E_r^{\text{TE}} = 0, H_r^{\text{TE}} = 0 \quad (51)$$

From Maxwell's equations in a source free medium we know that \mathbf{E} can be found from the curl of \mathbf{H} . We can then add up the terms, knowing where where the radial fields disappear. Assuming the normal plane wave time dependence and source-free space, we get that

$$E = E_r - ikc\epsilon_0 H_r \quad (52)$$

where k is the wave number and ϵ_0 the permittivity of free space. A corresponding argument is found for \mathbf{H} , so that the radial fields are all that is needed to fully describe the incoming fields. Put differently : the radial \mathbf{H} -field "contains" the angular \mathbf{E} -field, and vica verca. Expanding the TE and TM parts separately, one gets an expression for E

$$\psi_l = \psi_l(\bar{n}\alpha\varrho) \quad Y_{lm} = Y_{lm}(\theta, \varphi) \quad (53)$$

$$E_r = \frac{E_0}{\varrho^2} \sum_{l=1}^{\infty} \sum_{m=-l}^l l(l+1) A_{lm} \psi_l Y_{lm} \quad (54)$$

$$E_\theta = \frac{\alpha E_0}{\varrho} \sum_{l=1}^{\infty} \sum_{m=-l}^l \left[A_{lm} \psi'_l \partial_\theta Y_{lm} - \frac{m}{n_2^2} B_{lm} \psi_l \frac{Y_{lm}}{\sin(\theta)} \right]$$

$$E_\varphi = \frac{i\alpha E_0}{\varrho} \sum_{l=1}^{\infty} \sum_{m=-l}^l \left[A_{lm} \psi'_l \frac{Y_{lm}}{\sin(\theta)} - \frac{1}{n_2^2} B_{lm} \psi_l \partial_\theta Y_{lm} \right]$$

and the corresponding expansion for \mathbf{H} , in the same form, which can be found in the appendix of [22]. The shorthand in equation (53) are used from here on, to increase readability. The incoming fields are contained in the A_{lm}, B_{lm} coefficients

$$A_{lm} = \frac{1}{l(l+1)\psi_l(\alpha)} \int \frac{E_r^i}{E_0} Y_{lm}^*(\Omega) d\Omega \quad (55)$$

$$B_{lm} = \frac{1}{l(l+1)\psi_l(\alpha)} \int \frac{H_r^i}{H_0} Y_{lm}^*(\Omega) d\Omega \quad (56)$$

using the radial fields only. Note how the expansion contain the TE- and TM-terms, so that the field in the r -direction only have one term.

With magnetic fields perpendicular to electric ones, the factor difference can be written [15]

$$\mathbf{H}^i = -in_2\epsilon_0c\mathbf{E}^i, H_0 = \epsilon_0cE_0 \quad (57)$$

for the magnetic field. The integral for the B-coefficients is then only a complex factor different than that for the A-coefficients. This gives that

$$B_{lm} = -in_2A_{lm} \quad (58)$$

for this case. This leads to less coefficients to compute, but doesn't cut the computational complexity much, as these are fairly quick to calculate. It also allows us to focus solely on the electric field, which is done throughout this work.

We now have the incoming fields on a spherical harmonic basis. Note that since the magnetic permeability does not differ between the media, only the electric fields are needed to describe the scattering, and the magnetic fields come into it as a way to describe the electric fields. Placing the origin in the center of the sphere, we apply the boundary conditions over it.

2.3.3 Refraction and surface force density.

The refraction over the sphere changes the coefficients in equation 54. The fields outside the sphere are described by a combination of the scattered and incoming fields; these fields are not of interest, as the forces on the sphere are described by the field inside it. With the notation of Barton et.al. [22], we get

$$\psi_l = \psi_l(\bar{n}\alpha\rho), Y_{lm} = Y_{lm}(\theta, \varphi) \quad (59)$$

$$E_r^w = \frac{E_0}{\rho^2} \sum_{l=1}^{\infty} \sum_{m=-l}^l l(l+1)c_{lm}\psi_l Y_{lm} \quad (60)$$

$$E_\theta^w = \frac{\alpha E_0}{\rho} \sum_{l=1}^{\infty} \sum_{m=-l}^l \left[\bar{n}c_{lm}\psi_l' \partial_\theta Y_{lm} - \frac{d_{lm}}{n_2} m\psi_l \frac{Y_{lm}}{\sin(\theta)} \right]$$

$$E_\varphi^w = \frac{i\alpha E_0}{\rho} \sum_{l=1}^{\infty} \sum_{m=-l}^l \left[m\bar{n}c_{lm}\psi_l' \frac{Y_{lm}}{\sin(\theta)} - \frac{d_{lm}}{n_2} \psi_l \partial_\theta Y_{lm} \right]$$

$$c_{lm} = \frac{iA_{lm}}{\bar{n}^2\psi_l(\bar{n}\alpha)\xi_l^{(1)'} - \bar{n}\psi_l'(\bar{n}\alpha)\xi_l^{(1)}} \quad (61)$$

$$d_{lm} = \frac{iB_{lm}}{\psi_l(\bar{n}\alpha)\xi_l^{(1)'}(\alpha) - \bar{n}\psi_l'(\bar{n}\alpha)\xi_l^{(1)}} \quad (62)$$

where the c and d coefficients have been simplified from the expressions given by Barton et.al. [22]. This is used, but not mentioned, by Ellingsen [14], and discussed in an earlier article by Barton et.al [24]. The ξ -factors in the denominator simplify, compared to the expressions in [22], by using the Wronskian of the Ricatti-Bessel functions [25]:

$$\xi_n'(\alpha)\psi_n(\alpha) - \xi_n(\alpha)\psi_n'(\alpha) = i \quad (63)$$

This field can be plugged directly into equation (49). Taking the absolute value of a complex field, we multiply the field with the complex conjugate of itself. The expansion parameters used are (l, m) for the field, and (l', m') for the conjugated one. This yields the rather unwieldy equation:

$$\begin{aligned}
\sigma(\Omega) = & \frac{\epsilon_0 n_2^2 E_0^2}{4} (\bar{n}^2 - 1) \sum_{l=1}^{\infty} \sum_{l'=1}^{\infty} \sum_{m=-l}^l \sum_{m'=-l'}^l \\
& \times (l(l+1)l'(l'+1) c_{lm} c_{l'm'}^* \psi_l \psi_{l'} Y_{l,m} Y_{l',m'}^* \\
& + \alpha^2 [\bar{n}^2 c_{lm} c_{l'm'}^* \psi_l' \psi_{l'}' \partial_\theta Y_{l,m} \partial_\theta Y_{l',m'}^* \\
& - \frac{\bar{n}}{n_2} d_{lm} c_{l'm'}^* m \psi_l \psi_{l'}' \frac{Y_{lm}}{\sin(\theta)} \partial_\theta Y_{l',m'}^* \\
& - \frac{\bar{n}}{n_2} d_{l'm'}^* c_{lm} m' \psi_{l'} \psi_l' \frac{Y_{l',m'}^*}{\sin(\theta)} \partial_\theta Y_{lm} \\
& + \frac{1}{n_2^2} d_{lm} d_{l'm'}^* m m' \psi_l \psi_{l'}' \frac{Y_{lm} Y_{l',m'}^*}{\sin(\theta)^2}] \\
& + \alpha^2 [\bar{n}^2 m m' c_{lm} c_{l'm'}^* \psi_l' \psi_{l'}' \frac{Y_{l,m} Y_{l',m'}^*}{\sin(\theta)^2} \\
& - \frac{\bar{n}}{n_2} m c_{lm} d_{l'm'}^* \psi_l' \psi_{l'}' \partial_\theta Y_{l',m'}^* \frac{Y_{lm}}{\sin(\theta)} \\
& - \frac{\bar{n}}{n_2} m' c_{l'm'}^* d_{lm} \psi_l \psi_{l'}' \partial_\theta Y_{lm} \frac{Y_{l',m'}^*}{\sin(\theta)} \\
& + \frac{1}{n_2^2} d_{lm} d_{l'm'}^* \psi_l \psi_{l'}' \partial_\theta Y_{lm} \partial_\theta Y_{l',m'}^*]
\end{aligned} \tag{64}$$

where $\varrho = r/a \approx 1$ at the boundary, so that the ϱ -terms in equation (54) simply disappear at the boundary.

2.3.4 Power and Intensity

The equation for σ contains a term $\epsilon_0 n_2^2 E_0^2$, which describes the strength of the incoming fields. This will be rewritten in terms of the intensity [14], found by the average of the Poynting vector over the optical period

$$I = \langle \mathbf{E} \times \mathbf{H} \rangle_z = n_2 |E_x|^2 \epsilon_0 c \tag{65}$$

which simplifies to

$$I = n_2 E_0^2 \epsilon_0 c = I_0 \tag{66}$$

in the plane wave case.

Experimentally one typically quote the incoming intensity or power. The power is the integral of the intensity over a cross section of the entire beam. For comparisons between different beams, the effective power is used. This is the integral over the intensity over the droplet only. For a plane wave this simply becomes

$$P_{\text{eff}} = \pi a^2 I_0 \tag{67}$$

as the intensity is the same over the cross section of the sphere.

2.4 Organizing for numerical work.

2.4.1 Rewriting the surface force density.

The obtained expression for σ is unwieldy. Both Ellingsen [14] and Gouesbet [23] describe the algebra involved as tedious and time consuming. We start by writing out the spherical harmonics

$$Y_{lm}(\theta, \varphi) = \sqrt{\frac{2l+1}{4\pi} \frac{(l-m)!}{(l+m)!}} P_l^m(\cos \theta) e^{im\varphi} \quad (68)$$

where complex conjugation simply switches the sign in $e^{im\varphi}$. Some terms include the derivative in the θ -direction. The Legendre polynomials are dependent upon $u = \cos \theta$, and this substitution will be employed for the entire equation later. The chain rule gives

$$\frac{d}{d\theta} P_l^m(\cos \theta) = -\sin \theta \frac{d}{du} P_l^m(u) = -\sin \theta \partial_u P_l^m \quad (69)$$

so that the terms with the derivative of the Legendre Polynomials can be rewritten. Inserting this gives:

$$\begin{aligned} \sigma(\Omega) = & \frac{\epsilon_0 n_2^2 E_0^2}{4} (\bar{n}^2 - 1) \sum_{l=1}^{\infty} \sum_{l'=1}^{\infty} \sum_{m=-l}^l \sum_{m'=-l'}^{l'} (e^{i\varphi(m-m')}) \\ & \left(\sqrt{\frac{(2l+1)(l-m)!}{4\pi(l+m)!}} \sqrt{\frac{(2l'+1)(l'-m')!}{4\pi(l'+m')!}} \right) \\ & \times (l(l+1)l'(l'+1) c_{lm} c_{l'm'}^* \psi_l \psi_{l'} P_l^m P_{l'}^{m'} \\ & + \alpha^2 \bar{n}^2 c_{lm} c_{l'm'}^* \psi_l' \psi_{l'}' \sin^2 \theta \partial_u P_l^m \partial_u P_{l'}^{m'} \\ & + \alpha^2 \frac{\bar{n}}{n_2} d_{lm} c_{l'm'}^* m \psi_l \psi_{l'}' P_l^m \partial_u P_{l'}^{m'} \\ & + \alpha^2 \frac{\bar{n}}{n_2} d_{l'm'}^* c_{lm} m' \psi_{l'} \psi_l' P_{l'}^{m'} \partial_u P_l^m \\ & + \alpha^2 \frac{1}{n_2^2} d_{lm} d_{l'm'}^* m m' \psi_l \psi_{l'} \frac{P_l^m P_{l'}^{m'}}{\sin^2 \theta} \\ & + \alpha^2 \bar{n}^2 m m' c_{lm} c_{l'm'}^* \psi_l' \psi_{l'}' \frac{P_l^m P_{l'}^{m'}}{\sin^2 \theta} \\ & + \alpha^2 \frac{\bar{n}}{n_2} m c_{lm} d_{l'm'}^* \psi_l' \psi_{l'}' \partial_u P_{l'}^{m'} P_l^m \\ & + \alpha^2 \frac{\bar{n}}{n_2} m' c_{l'm'}^* d_{lm} \psi_l \psi_{l'}' \partial_u P_l^m P_{l'}^{m'} \\ & + \alpha^2 \frac{1}{n_2^2} d_{lm} d_{l'm'}^* \psi_l \psi_{l'} \sin^2 \theta \partial_u P_l^m \partial_u P_{l'}^{m'} \end{aligned} \quad (70)$$

Many of these terms are equal, or similar. They are obtained by the similar expansions of the electric field, which makes this somewhat intuitive. Let us start with the terms with dependence upon the Legendre Polynomials and θ , as these will constitute the main numerical work

$$\begin{aligned}
\sigma(\Omega) &= \frac{\epsilon_0 n_2^2 E_0^2}{4} (\bar{n}^2 - 1) \sum_{l=1}^{\infty} \sum_{l'=1}^{\infty} \sum_{m=-l}^l \sum_{m'=-l'}^l (e^{i\varphi(m-m')}) \\
&\quad \left(\sqrt{\frac{(2l+1)(l-m)!}{4\pi(l+m)!}} \sqrt{\frac{(2l'+1)(l'-m')!}{4\pi(l'+m')!}} \right) \\
&\quad \times (l(l+1)l'(l'+1)c_{lm}c_{l'm'}^* \psi_l \psi_{l'} P_l^m P_{l'}^{m'} \\
&\quad + \alpha^2 \sin^2 \theta \partial_u P_l^m \partial_u P_{l'}^{m'} (\bar{n}^2 c_{lm} c_{l'm'}^* \psi_l' \psi_{l'}' + \frac{1}{n_2^2} d_{lm} d_{l'm'}^* \psi_l \psi_{l'}) \\
&\quad + \alpha^2 m m' \frac{P_l^m P_{l'}^{m'}}{\sin^2 \theta} \left(\frac{1}{n_2^2} d_{lm} d_{l'm'}^* + \bar{n}^2 c_{lm} c_{l'm'}^* \psi_l' \psi_{l'}' \right) \\
&\quad + \alpha^2 m \frac{\bar{n}}{n_2} P_l^m \partial_u P_{l'}^{m'} (d_{lm} c_{l'm'}^* \psi_l \psi_{l'}' + c_{lm} d_{l'm'}^* \psi_l' \psi_{l'}) \\
&\quad + \alpha^2 m' \frac{\bar{n}}{n_2} \partial_u P_l^m P_{l'}^{m'} (d_{l'm'}^* c_{lm} \psi_l \psi_{l'}' + c_{l'm'}^* d_{lm} \psi_l \psi_{l'}')
\end{aligned} \tag{71}$$

$$\tag{72}$$

2.4.2 Expansion of the formalism: use of associated Legendre Polynomials.

Equation (18) gives the coefficients needed for the surface motion. Consider the φ -dependence, where σ is a combination of expansions in spherical harmonics. The constants have no dependence on φ , which leaves

$$\sigma_{l_\sigma, m_\sigma} = \int_0^{2\pi} e^{i\varphi(-m_\sigma + m - m')} d\varphi \times \dots \tag{73}$$

ignoring the rest of the equation for now. This has the same result seen earlier, that the exponent must be zero to ensure a non-zero result. We can thus write out

$$\sigma_{l_\sigma, m_\sigma} = \begin{cases} 2\pi \times \dots & \text{if } m_\sigma = m - m' \\ 0 & \text{otherwise} \end{cases} \tag{74}$$

for the terms in m . This leaves an integral over u , so that:

$$\sigma_{l_\sigma, m_\sigma} = \frac{(2l_\sigma + 1)(l_\sigma - m_\sigma)!}{4\pi(l_\sigma + m_\sigma)!} \sum_{l=1}^{\infty} \sum_{l'=1}^{\infty} \sum_{m=-l}^l \sum_{m'=-l'}^l 2\pi \delta_{m_\sigma, (m-m')} \quad (75)$$

$$\times \frac{\epsilon_0 n_2^2 E_0^2}{4} (\bar{n}^2 - 1) \sqrt{\frac{(2l+1)(l-m)!}{4\pi(l+m)!}} \sqrt{\frac{(2l'+1)(l'-m')!}{4\pi(l'+m')!}} \quad (76)$$

$$\times \int_{-1}^1 du [P_l^m P_{l'}^{m'} P_{l_\sigma}^{m_\sigma} (l(l+1)l'(l'+1)c_{lm}c_{l'm'}^* \psi_l \psi_{l'} \quad (77)$$

$$+ \alpha^2(1-u^2)\partial_u P_l^m \partial_u P_{l'}^{m'} P_{l_\sigma}^{m_\sigma} (\bar{n}^2 c_{lm}c_{l'm'}^* \psi_l' \psi_{l'}' + \frac{1}{n_2^2} d_{lm}d_{l'm'}^* \psi_l \psi_{l'})$$

$$+ \alpha^2 m m' \frac{P_l^m P_{l'}^{m'}}{(1-u^2)} P_{l_\sigma}^{m_\sigma} (\frac{1}{n_2^2} d_{lm}d_{l'm'}^* + \bar{n}^2 c_{lm}c_{l'm'}^* \psi_l' \psi_{l'}')$$

$$+ \alpha^2 m \frac{\bar{n}}{n_2} P_l^m \partial_u P_{l'}^{m'} P_{l_\sigma}^{m_\sigma} (d_{lm}c_{l'm'}^* \psi_l \psi_{l'}' + c_{lm}d_{l'm'}^* \psi_l' \psi_{l'})$$

$$+ \alpha^2 m' \frac{\bar{n}}{n_2} \partial_u P_l^m P_{l'}^{m'} P_{l_\sigma}^{m_\sigma} (d_{l'm'}^* c_{lm} \psi_l \psi_{l'}' + c_{l'm'}^* d_{lm} \psi_l \psi_{l'}')] \quad (78)$$

Observe line 4 and 5 in this equation, they share coefficients; similarly line 6 and 7 share coefficients. These can be combined. Defining some more coefficients a more tractable version is obtained:

$$\sigma_{l_\sigma, m_\sigma} = \frac{\epsilon_0 n_2^2 E_0^2}{4} (\bar{n}^2 - 1) \sum_{l=1}^{\infty} \sum_{l'=1}^{\infty} \sum_{m=-l}^l \sum_{m'=-l'}^l \delta_{m_\sigma, (m-m')} \quad (79)$$

$$\begin{aligned} & \times K [I \times c_{lm}c_{l'm'}^* \psi_l \psi_{l'} \\ & + M\alpha^2 (\bar{n}^2 c_{lm}c_{l'm'}^* \psi_l' \psi_{l'}' + \frac{1}{n_2^2} d_{lm}d_{l'm'}^* \psi_l \psi_{l'}) \\ & + N\alpha^2 \frac{\bar{n}}{n_2} (d_{lm}c_{l'm'}^* \psi_l \psi_{l'}' + c_{lm}d_{l'm'}^* \psi_l' \psi_{l'})] \end{aligned}$$

$$K = \frac{(2l_\sigma + 1)(l_\sigma - m_\sigma)!}{2(l_\sigma + m_\sigma)!} \sqrt{\frac{(2l+1)(l-m)!}{4\pi(l+m)!}} \sqrt{\frac{(2l'+1)(l'-m')!}{4\pi(l'+m')!}} \quad (80)$$

$$I = \int_{-1}^1 du l(l+1)l'(l'+1)P_l^m P_{l'}^{m'} P_{l_\sigma}^{m_\sigma} \quad (81)$$

$$M = \int_{-1}^1 du ((1-u^2)\partial_u P_l^m \partial_u P_{l'}^{m'} P_{l_\sigma}^{m_\sigma} + m m' \frac{P_l^m P_{l'}^{m'}}{(1-u^2)} P_{l_\sigma}^{m_\sigma})$$

$$N = \int_{-1}^1 du (m P_l^m \partial_u P_{l'}^{m'} P_{l_\sigma}^{m_\sigma} + m' \partial_u P_l^m P_{l'}^{m'} P_{l_\sigma}^{m_\sigma})$$

The unwieldy equation (70) is thus cut into smaller portions, that can be dealt with. The coefficients in equations (80) and (81) are independent on the parameters of the system, as long as the assumptions hold: as per the lack of system dependent parameters n, α, c, d . These

constitute the main computational challenge, and can luckily be reused for different droplet systems.

Notice that this equation holds as long as the fields are the same for the duration of the pulse. The rise and fall of the intensity is dealt with in the fluid mechanics. This means that equation (79) holds with a different pulse behaviour, for example the rise and fall times described by Brevik and Kluge [13].

This holds no matter the symmetry of the incoming beam(s). A symmetry is most helpful for the numerical work, as well as expected. It will typically manifest itself as disappearing terms of c, d for certain m, m' .

Applying the fluid mechanical treatment, one obtains that

$$h_{l,m}(\infty) = \frac{a^2}{\gamma} \frac{1}{l^2 + l - 2} \frac{\epsilon_0 n_2^2 E_0^2}{4} (\bar{n}^2 - 1) \sum \dots \quad (82)$$

where the contents of the sums are ignored.

2.4.3 Computational complexity

The bulk of the numerical work are the coefficients in equation (81). These can, handily, be calculated once and reused for different droplet systems. The condition for a good approximation is that the values of l, l', l_σ all be truncated at a maximum value of $maxL \approx \alpha$. Thus the numerical load is increased with larger droplets, until the limit for geometrical optics is found.

The sums in (79) has a total number of terms in l :

$$T(\alpha) \approx l'l_\sigma = \mathcal{O}(\alpha^3) \quad (83)$$

where the values of m is not yet taken into account.

If the values of m were allowed to be chosen freely, they would multiply the number of terms with another α^3 . This is not the case, however, as the integral over φ is non-zero over only certain values. Consider the case where l, l' have the same value, say 3, and m_σ is 0. Since the condition is that

$$m - m' = m_\sigma \implies m = m' \quad (84)$$

we are simply limited to the $2l+1$ combinations of equal m, m' . Unequal l, l' , e.g. 2, 3, will naturally have no extra way of combining that a corresponding equal pair, e.g. 3, 3 has. Thus the number of terms has to be $l + l' + 1$ or less. With big O-notation, this gives an additional $\mathcal{O}(maxL)$ terms per set of values for l . The total number of terms increases to

$$T(\alpha) = \mathcal{O}(\alpha^3) * \mathcal{O}(\alpha) = \mathcal{O}(\alpha^4) \quad (85)$$

albeit with a smaller constant factor.

The polynomial behaviour of the total number of terms are found. Each term will require specific values of the integrals found in equation (81). These are, however, not linear in l , as the Legendre polynomials

grow larger with l . Consider their definition

$$\begin{aligned} P_l^m &= (1-x^2)^{\frac{m}{2}} \frac{d^{(l+m)}}{dx^{(l+m)}} (1-x^2)^l \\ &= (1-x^2)^{\frac{m}{2}} \frac{d^{(l+m)}}{dx^{(l+m)}} [x^{2(l-0)} + x^{2(l-1)} \dots + x^{2(l-l)}] \end{aligned} \quad (86)$$

where the constants have been ignored, for clarity. This is a polynomial with roughly $l/2$ terms, as one half is removed by the differentiation. With a non-zero m , some more terms become zero by the differentiation, but the expression is multiplication of a new polynomial. All in all we end up with a number of terms linear in l .

With the three Legendre polynomials in the integrands in (81), they form a polynomial with a number of terms of order $\mathcal{O} = \alpha^3$. These need to be calculated for all the different combinations found earlier, ending with a polynomial run time of

$$T(\alpha) = \mathcal{O}(\alpha^7) \quad (87)$$

which can be reused for different systems. If the beam profile has symmetries, so that A, B are non-zero only for specific m , it is reduced to

$$T(\alpha) = \mathcal{O}(\alpha^6) \quad (88)$$

in most specific cases. Note that the largest saving in time comes by recognizing that $m_\sigma = m - m'$, reducing the run time by two orders in α .

The run time quickly becomes forbidding with higher α . The different terms are not independent upon each other. This indicates that this system could be parallelized quite effectively. Once the coefficients in (81) are calculated, the results for different systems could be found, with a significant lower run time.

2.5 Different cases for the incoming fields

2.5.1 Single plane wave, or Gaussian beam, with circular polarization.

This is the case described in figure 3, investigated in a recent article by Ellingsen [14]. The Gaussian beam is typically used to describe a "perfect" laser beam, and can thus be a practical approximation of the incoming beam. Taking the limit where the beam waste approaches infinity, plane wave case is handily obtained.

The electromagnetic fields of the Gaussian wave have no simple, closed form expression, i.e. we describe them by a sum with an infinite number of terms. The expansion parameter used here is

$$s = \frac{1}{kw_0} = \frac{1}{\kappa} \quad (89)$$

where k is the wave number. These can be described to many orders of s , and give a good approximation for as long as s is small. The expressions used are the ones given by Davis [26], with the formalism

of Barton et.al. [24] as used by Ellingsen [14]. These are all equivalent, bar the details of nomenclature. To leading order in s

$$E_x^i = E_0 \psi_0^* e^{ikz}, \quad E_y^i = iE_x^i, \quad E_z^i = \frac{2Q^*}{kw_0^2}(x + iy) \quad (90)$$

with

$$\psi_0 = iQ e^{-iQ(x^2+y^2)/w^2}, \quad Q = \frac{1}{2i/kw^2} \quad (91)$$

for the usual Cartesian coordinates (x, y, z) . More detail on the choice of expansion parameter can be found in ref [23]. The magnetic field can be expressed as

$$\mathbf{H}^i = -\frac{in_2}{\mu_0 c} \mathbf{E}^i \quad (92)$$

as described earlier, which simplify the expressions for the spherical harmonic expansion parameters. Correspondingly, the further treatment will focus on the electrical field.

Assuming a small expansion parameter s restricts the theory to regions where

$$\kappa \gg 0 \quad (93)$$

or

$$\kappa^2 \gg \alpha \implies \frac{\lambda_0}{w_0} \ll 2\pi n_2 \frac{w_0}{a} \quad (94)$$

so that the approximation of the beam holds over the droplet [14]. The important parameters for the applicability are thus wavelength, radius and beam waist. Take the case with an $a = 2\mu m$ droplet, illuminated by a beam with $\lambda = 1064nm$ this becomes

$$w_0 \gg 0.5\mu m \quad (95)$$

while definitely being a significant portion of the radius, is still small enough to be of use.

Consider the radial electric field in spherical coordinates

$$E_r^i = E_x^i \sin \theta e^{i\varphi} + \cos \theta E_z^i \quad (96)$$

needed for the expansion of the fields. Working to leading order in s , using the series expansion of the exponential, we get [14]

$$\frac{E_r^i}{E_0} = \frac{\kappa^4 \sin \theta}{(\kappa^2 + 2ia \cos \theta)^2} \exp \left[\frac{i\alpha \kappa^2 \cos \theta - \alpha^2 (1 + \cos^2 \theta)}{\kappa^2 + 2ia \cos \theta} \right] e^{i\varphi} \quad (97)$$

for the electric field. This is inserted into equation (61), to get the expansion parameters. The integral over φ can easily be done

$$\int_0^{2\pi} e^{i\varphi(1-m)} d\varphi = 2\pi \delta_{m,1} \quad (98)$$

where δ is the Kroenecker delta. The φ -part thus selects $m = 1$ -terms only. This is consistent with the plane wave expansions found in

Jackson [20]. Following the nomenclature used by Ellingsen [14]

$$A_{lm} = \frac{1}{l(l+1)\psi_l} \int \frac{E_r}{E_0} Y_{lm}^*(\Omega) d\Omega \quad (99)$$

$$= \frac{\sqrt{(2l+1)}\sqrt{\pi}}{[l(l+1)]^{\frac{3}{2}}} \Phi_l$$

$$\Phi_l(\alpha, \kappa) = \int_{-1}^1 du \frac{\kappa^4 \sqrt{(1-u^2)} P_l^1}{(\kappa^2 + 2i\alpha u)^2} \exp\left[\frac{i\alpha\kappa^2 u - \alpha^2(1+u^2)}{\kappa^2 + 2i\alpha u}\right] \quad (100)$$

with the usual substitution in u . This is then calculated numerically. The plane wave case simplifies it enough for an analytical solution [14]

$$\Phi_l = \frac{2^{l+1}}{\alpha^2} l(l+1) \psi_l(\alpha) \quad (101)$$

where the l -dependence is recognized as the same as the one described in Jackson [20]. With the new dependence on m , equation (79) can be rewritten as:

$$\sigma_{l\sigma,0} = \frac{\epsilon_0 n_2^2 E_0^2}{4} (\bar{n}^2 - 1) \sum_{l=1}^{\infty} \sum_{l'=1}^{\infty} \quad (102)$$

$$\times K \left[\mathbf{I} \times c_l c_{l'}^* \psi_l \psi_{l'} \right. \\ \left. + M \alpha^2 (\bar{n}^2 c_l c_{l'}^* \psi_l' \psi_{l'}' + \frac{1}{n_2^2} d_l d_{l'}^* \psi_l \psi_{l'}) \right. \\ \left. + N \alpha^2 \frac{\bar{n}}{n_2} (d_l c_{l'}^* \psi_l \psi_{l'}' + c_l d_{l'}^* \psi_l' \psi_{l'}) \right]$$

$$K = \frac{(2l_\sigma + 1)}{2} \frac{1}{l_\sigma(l_\sigma + 1)} \sqrt{\frac{(2l+1)}{4\pi l(l+1)}} \sqrt{\frac{(2l'+1)}{4\pi l'(l'+1)}} \quad (103)$$

$$I = \int_{-1}^1 du l(l+1)l'(l'+1) P_l^1 P_{l'}^1 P_{l_\sigma} \quad (104)$$

$$M = \int_{-1}^1 du ((1-u^2) \partial_u P_l^1 \partial_u P_{l'}^1 P_{l_\sigma} + \frac{P_l^1 P_{l'}^1}{(1-u^2)} P_{l_\sigma})$$

$$N = \int_{-1}^1 du (P_l^1 \partial_u P_{l'}^1 P_{l_\sigma} + \partial_u P_l^1 P_{l'}^1 P_{l_\sigma})$$

$$K = \frac{(2l_\sigma + 1)}{2} \frac{1}{l_\sigma(l_\sigma + 1)} \sqrt{\frac{(2l+1)}{4\pi l(l+1)}} \sqrt{\frac{(2l'+1)}{4\pi l'(l'+1)}} \quad (105)$$

This could, in principle, be solved numerically to find the perturbations, and yield the same results as found in [14]. Making sure this will fit with the equations found there, will however be a good test to the work done so far.

From here on the formalism of [14,27] will be applied; using m, n in place of l, l' in the incoming fields (as the m, m' are fixed to one value). The expansion $\sigma_{l_\sigma, m_\sigma}$ will then be σ_l , with $m_\sigma = 0$. The refracted

expansion coefficients c, d are changed as well, using the description in equation (99). The old c, d can be written as

$$c_{\text{old}} = \sqrt{\frac{\pi(2l+1)}{[l(l+1)]^3}} c_{\text{new}} \quad (106)$$

$$d_{\text{old}} = -in_2 \sqrt{\frac{\pi(2l+1)}{[l(l+1)]^3}} d_{\text{new}}$$

expressed by the new ones. These new definitions are inserted into the equations for σ . Note that the extra $-in_2$ for d is handled in equation (102), with an extra negative sign if $i^* = -i$. The l, l' -terms are the same for all combinations of c, d , and are handled in K . This gives

$$K = \frac{1}{8} \frac{(2l+1)(2m+1)(2n+1)}{[m(m+1)n(n+1)]^2} \quad (107)$$

which certainly looks neater. The constant $1/8$ -part is taken into equation (102), while the rest is applied to equation (104). The integrand in the N-terms are rewritten with the chain rule, for easier numerical work. After this step, the same result as in [14] are obtained:

$$\sigma_l = \frac{\epsilon_0 n_2^2 E_0^2 (\bar{n}^2 - 1)}{32} \sum_{m=1}^{\infty} \sum_{n=1}^{\infty} c_m c_n^* \psi_m \psi_n I_{lmn} \quad (108)$$

$$+ \alpha^2 [c_m c_n^* \psi'_m \psi'_n + d_m d_n^* \psi_m \psi_n] M_{lmn}$$

$$+ \alpha^2 [c_m d_n^* \psi'_m \psi_n - d_m c_n^* \psi_m \psi'_n] N_{lmn}$$

$$I_{lmn} = \frac{(2l+1)(2m+1)(2n+1)}{[m(m+1)n(n+1)]} \int_{-1}^1 du P_l^0 P_m^1 P_n^1 \quad (109)$$

$$M_{lmn} = \frac{(2l+1)(2m+1)(2n+1)}{[m(m+1)n(n+1)]^2}$$

$$\times \int_{-1}^1 du P_l^0 [(1-u^2) P_m^{1'} P_n^{1'} + \frac{P_m^1 P_n^1}{1-u^2}]$$

$$N_{lmn} = \frac{(2l+1)(2m+1)(2n+1)}{[m(m+1)n(n+1)]^2} \int_{-1}^1 du P_l^{0'} P_m^1 P_n^1$$

Values of I, M, N for l up to 50 were obtained from Ellingsen, along with his corresponding scripts in Mathematica. These were used in the early numerical work, and were a great help for writing similar programs for the other case.

2.5.2 Plane waves from opposite sides of the droplet.

Take the case of an incoming plane wave with electric field

$$E_x^{\text{left}} = E_0 e^{ikz}, E_y^{\text{left}} = iE_x^{\text{left}} \quad (110)$$

that propagates along the z -axis (from the left). Imagine that this beam has been split, and an identical beam is sent from the opposite side, propagating along $-z$. This flips the sign of the wave vector, as the

beam travels in the opposite direction. In order to conserve helicity, one also needs to flip the sign in either E_x or E_y . This gives an incoming wave from the right

$$E_x^{\text{right}} = E_0 e^{-ikz}, E_y^{\text{right}} = -iE_x^{\text{right}} \quad (111)$$

with the same polarization as the left one. The same result can be found by writing out the incoming beam as a vector, and doing a rotation around the x-axis. The optical cables transporting the beams may not be exactly the same number of wavelengths long. In that case a phase difference is introduced so that

$$E^{\text{right}} = E^{\text{right}} e^{i\eta}, E^{\text{left}} = E^{\text{left}} e^{i\eta} \quad (112)$$

for an angle η . The total incoming electric field becomes the sum of the fields coming from the left and right side. The total incoming radial field is then found

$$E_r^i = E_0 \sin(\theta) (e^{i\kappa \cos(\theta)} e^{i\varphi} + e^{-i\kappa \cos(\theta)} e^{-i\varphi}) \quad (113)$$

using equation (96) and that $kz = kr \cos(\theta) = \alpha \cos(\theta)$ at the droplet boundary.

This field is inserted into the expression for the expansion parameter A :

$$\begin{aligned} A_{lm} &= \frac{1}{l(l+1)\psi_l(\alpha)} \int \frac{E_r^i}{E_0} Y_{lm}^*(\Omega) d\Omega \\ &= \frac{1}{l(l+1)\psi_l} \sqrt{\frac{(2l+1)(l-m)!}{4\pi(l+m)!}} \\ &\quad \times \int_0^{2\pi} d\varphi \int_{-1}^1 du \sqrt{1-u^2} P_l^m(u) e^{-im\varphi} (e^{i\kappa u} e^{i\varphi} + e^{-i\kappa u} e^{-i\varphi}) \end{aligned} \quad (114)$$

where the usual parameter $u = \cos(\theta)$ is used. The φ is easily solved

$$\begin{aligned} A_{lm} &= \frac{1}{l(l+1)\psi_l} \sqrt{\pi(2l+1) \frac{(l-m)!}{(l+m)!}} \\ &\quad \times \int_{-1}^1 du \sqrt{1-u^2} P_l^m(u) (e^{i\kappa u} \delta_{m,1} + e^{-i\kappa u} \delta_{m,-1}) \end{aligned} \quad (115)$$

where the φ -integral has selected values for m . This is the integral used in the numerical calculations. Certain properties of the Legendre polynomials [20]

$$P_l^{-m} = (-1)^m \frac{(l-m)!}{(l+m)!} P_l^m, P_l^m(-u) = (-1)^{l+m} P_l^m(u) \quad (116)$$

can be used to massage the case for $m = -1$, and better display the result. This simplifies the coefficients to:

$$\begin{aligned} A_{lm} &= A_l (\delta_{m,1} + (-1)^{l+1} \delta_{m,-1}) \\ A_l &= \frac{1}{l(l+1)\psi_l} \sqrt{\pi(2l+1) \frac{(l-m)!}{(l+m)!}} \int_{-1}^1 e^{i\kappa u} P_l^1 \sqrt{1-u^2} du \end{aligned} \quad (117)$$

We thus have a field with non-zero coefficients for $m = \pm 1$. In the surface force, equation (75), the m -dependence is given as

$$\delta_{m_\sigma, (m' - m)} \quad (118)$$

where m'/m in this case is limited to ± 1 . This limits the values of m_σ to $0, \pm 2$. This leads to different values for the coefficients in equation (81), as values for $m_\sigma \pm 2$ needs to be calculated.

Since the incoming beams are plane waves, the intensity is described by equation (66). The droplet is radiated by two beams, doubling the effective power, so that

$$n_2 E_0^2 \epsilon_0 = \frac{I_0}{c} = \frac{P_{\text{eff}}}{2\pi a^2 c} \quad (119)$$

which is readily used in the expression for the force density. Inserting into equation (79) gives that

$$\sigma_{l_\sigma, m_\sigma} = \frac{\epsilon_0 n_2^2 E_0^2}{4} (\bar{n}^2 - 1) \dots = \frac{P_{\text{eff}} n_2}{8\pi a^2 c} (\bar{n}^2 - 1) \sum \dots \quad (120)$$

so that the surface perturbations become

$$h_{l, m}(\infty) = P_{\text{eff}} \frac{1}{\gamma(l^2 + l - 2)} \frac{n_2}{8\pi c} (\bar{n}^2 - 1) \sum \dots \quad (121)$$

3 Numerical calculations

Scripts were written to calculate the droplet shapes of the different cases. These shapes are the starting points for perturbations that appear when the beam is turned off. The Mathematica code can be found in appendices A through C.

Following the approach used in [14], two cases are investigated. A droplet with air and water, and an oil emulsion with very low surface tension, such as the one used in the optical sculpting work of Ward et.al. [4]. The relevant system dependent variables are the refractive indices and the surface tension, given in Table 1.

Table 1: Physical parameters for the different cases.

Case	n_1	n_2	γ N/m
Water and air	1.33	1	$73 \cdot 10^{-3}$
Oil emulsion	1.41	1.33	$50 \cdot 10^{-6}$

3.1 Plane wave and Gaussian wave from one side.

Using these variables gives the droplets given in figure 4 for the static case. They display the same deformations as the similar figures in [14]. In the transient case, these shapes can be imagined as an initial displacement in the equation for h .

Notice the difference in effective power needed to deform the droplets in the different cases. The large difference in surface tension between the oil emulsion and the water results in a difference in effective power of roughly the same order.

The water-air droplet has higher optical contrast than the oil emulsion. This is clearly seen in the deformations, in the way the tip of the displacement is sharp, also for the plane wave case. The droplet is so good at bending the light that the plane wave case has a more distinct deformation with the same effective power! The lower optical contrast in the oil emulsion is clearly shown in the difference in shape between the droplets, with the plane wave droplet approaches more of a square in shape.

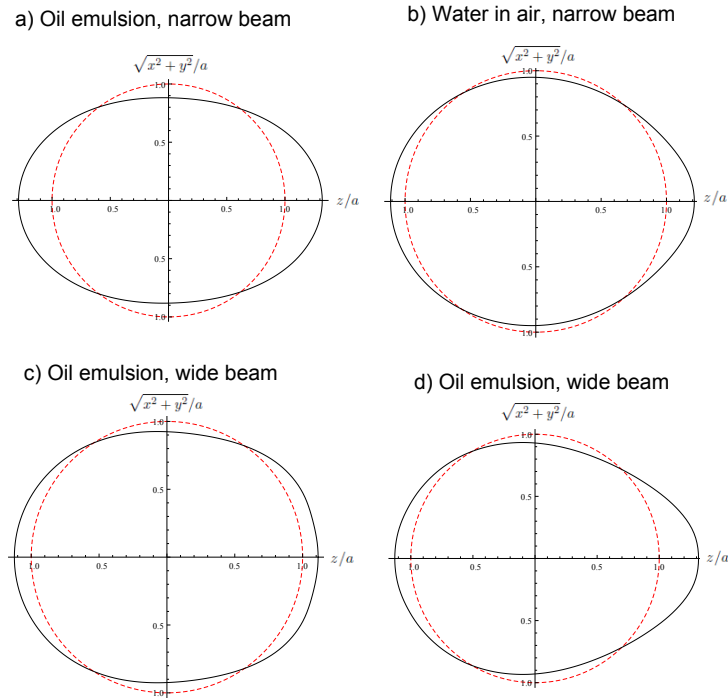


Figure 4: Droplet deformation for the static case, for droplets as given in table (1). The narrow beam has a beam waist of $\omega_0 = 1,5\mu m$. The effective powers are chosen to provide examples with deformations, and are 7 mW in a), 28 mW in c) and 70W in both b) and d).

3.2 Plane wave beams from both sides.

Writing the code for the numerical treatment of this case turned out to be more involved than anticipated. The code still have some issues. Changing the parameters to the water in air case, does for example make the required input powers unreasonably large. The convergence of the series also seem to be problematic for some input parameters, giving strange results between different maximum values of l .

There might a normal programming bug, or a number of them, in the code. Another possibility is the stability of the numerical calculations. There are a number of integrals that should return zero. These contains integrands of highly oscillatory functions. Rewriting the program once again, while going over the "NIntegrate" function in more detail would be a logical next step.

The oil emulsion case does give some plausible results. The shape is consistently obtained, no matter the other problems when working with the code. Figure 6 shows the droplet shape obtained. The droplet is less symmetric than earlier, being rotationally symmetric in θ , but not in φ . This difference can clearly be seen in Figure 5.

The displacements are of the same magnitude as those found for the one sided case in Figure 4. The shape is more pointed. Considering that the beams on both sides of the droplet have been focused by the droplet "lens", this seems reasonable. The general shape also fits the

one found in the optical sculpting work by Ward et.al., see Figure 1.

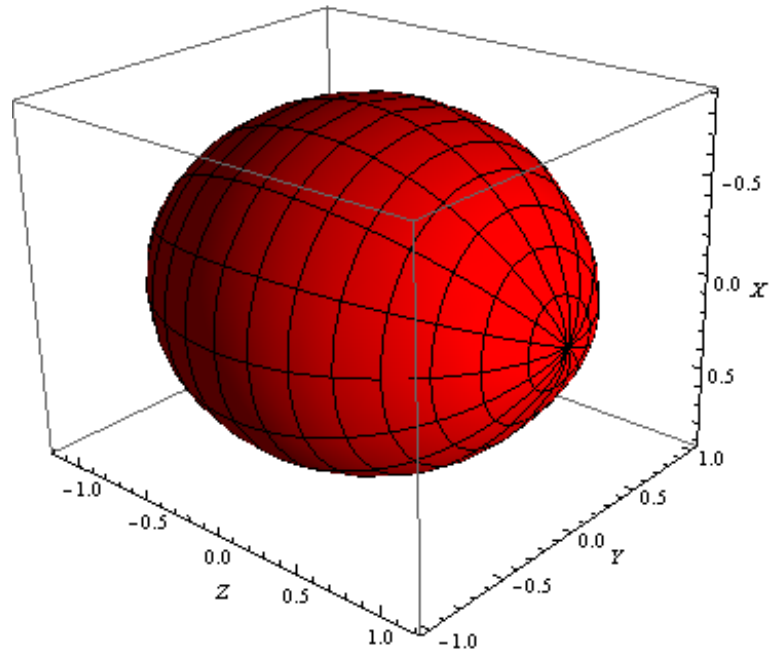


Figure 5: Droplet deformation for the oil emulsion case, in a 3 dimensional plot. The effective power is of $28mW$, as with the similar plots in Figure 4.

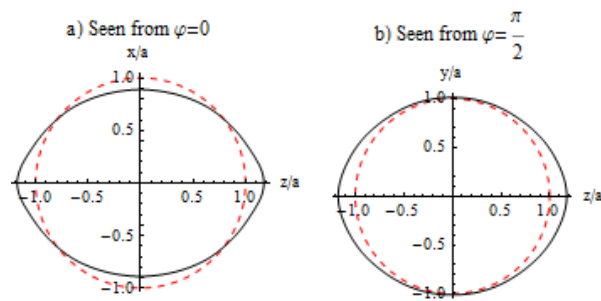


Figure 6: Droplet deformation for the oil emulsion case. The same shape as in Figure 6, with set values of φ .

4 Discussion and conclusion

A framework for the behaviour of micrometer sized droplets under influence of a laser beam was presented. The theory presented is not dependent upon any particular beam symmetry. In particular, equation (79) is a generalized version of similar expressions found in earlier work.

The generalization of the theory proved more difficult to do than anticipated. The calculations are quite involved, and the articles on the subject concise. Expanding to incoming beams from both sides, in particular, proved it necessary to change a surprising amount of theory.

The special case of a single Gaussian, or plane wave, beam was investigated, the equations simplified to account for symmetries in this case. A mathematica script was written to calculate the deformations of a $2\mu\text{m}$ droplet, for the Gaussian and plane wave case. The results confirm that the theory works for these test cases.

Similarly, a script was written to describe the case with plane waves from opposite sides of the droplet. Getting the numerics to work smoothly was difficult, returning problematic values. Much time was spent hunting for bugs, and rewriting the script from scratch. The script may still contain regular programming bugs, or there may be a problem with the accuracy of the numerics used.

Reasonable shapes of the droplet was found, for the case of a plane wave beams from either side on an oil emulsion system. These shapes fit well with results for similar systems. Interestingly, the droplet showed markedly different symmetries than with the single beam case.

References

- [1] D.G. Grier. A revolution in optical manipulation. *Nature*, 424:810–816, 2003.
- [2] G.C. Spalding M. P. MacDonald and K. Dholakia. Microfluidic sorting in an optical lattice. *Nature*, 426:421–424, 2003.
- [3] T. J. Moon C. C. Cunningham J. Guck, R. Ananthakrishnan and J. Käs. Optical deformability of soft biological dielectrics. *Phys. Rev. Lett.*, 84:5451–5454, 2000.
- [4] C.D. Mellor A.D. Ward, M.G. Berry and C.D. Bain. Optical sculpture: controlled deformation of emulsion droplets with ultralow interfacial tensions using optical tweezers. *Chem. Commun.*, pages 4515–4517, 2006.
- [5] J. Ng J. Chen, Z. Lin, and C.T. Chan. Optical pulling force. *Nature Photonics*, 5:531–534, 2011.
- [6] J.J. Saenz. Optical forces: Laser tractor beams. *Nature Photonics*, 5:514–515, 2011.
- [7] P. Abgrall and A.M. Gué. Lab-on-chip technologies: making a microfluidic network and coupling it into a complete microsystem—a review. *Journal of Micromechanics and Microengineering*, 17:R15, 2007.

- [8] D. Psaltis Z. Li. Optofluidic dye lasers. *Microfluidics and Nanofluidics*, 4:145–158, 2008.
- [9] M. R. Vincent C.N. Baroud and J.P. Delville. An optical toolbox for total control of droplet microfluidics. *Lab Chip*, 7:1029–1033, 2007.
- [10] X. Lei B. Chen W. Wang D. Liu, G. Liang and X. Zhou. Highly efficient capillary polymerase chain reaction using an oscillation droplet microreactor. *Analytica Chimica Acta*, 718:58 – 63, 2012.
- [11] J. Zhang and Richard K. Chang. Shape distortion of a single water droplet by laser-induced electrostriction. *Opt. Lett.*, 13:916–918, 1988.
- [12] K. L. Poon H. M. Lai, P. T. Leung and K. Young. Electrostrictive distortion of a micrometer-sized droplet by a laser pulse. *J. Opt. Soc. Am. B*, pages 2430–2437, 1989.
- [13] I. Brevik and R. Kluge. Oscillations of a water droplet illuminated by a linearly polarized laser pulse. *J. Opt. Soc. Am. B*, 16:976–985, 1999.
- [14] S. Å. Ellingsen. Theory of microdroplet and microbubble deformation by gaussian laser beam. *J. Opt. Soc. Am. B*, 30:1694–1710, 2013.
- [15] S. Å. Ellingsen. Microdroplet oscillations during optical pulling. *Phys. Fluids*, 24:022002, 2012.
- [16] G. Whyte L. Boyde, A. Ekpenyong and J. Guck. Comparison of stresses on homogeneous spheroids in the optical stretcher computed with geometrical optics and generalized lorenz-mie theory. *Appl. Opt.*, 51(33):7934–7944, 2012.
- [17] S. Å. Ellingsen and I. Brevik. Electrostrictive counterforce on fluid microdroplet in short laser pulse. *Opt. Lett.*, 37:1928–1930, 2012.
- [18] I. Brevik. Experiments in phenomenological electrodynamics and the electromagnetic energy-momentum tensor. *Physics Reports*, 52(3):133 – 201, 1979.
- [19] S.Å.Ellingsen. Surface waves on a bubble or droplet, 2013. Compendium for the course EP8402 at NTNU.
- [20] J. D. Jackson. *Classical Electrodynamics*. Wiley, 1998.
- [21] S. Chandrasekhar. *Hydrodynamic and Hydromagnetic stability*. Oxford University press., 1961.
- [22] D.R. Alexander J.P Barton and S.A. Schaub. Theoretical determination of net radiation force and torque for a spherical particle illuminated by a focused laser beam. *Journal of Applied Physics*, (10):4594–4602, 1989.
- [23] G. Gouesbet and G. Gréhan. *Generalized Lorenz-Mie Theory*. Springer, 2011.
- [24] D.R Alexander J.P Barton and S.A. Schaub. Internal and near surface electromagnetic fields for a spherical particle irradiated by a focused laser beam. *Journal of Applied Physics*, 64:1632–1639, 1988.
- [25] M. Abramowitz and I.A. Stegun. *Handbook of Mathematical functions*. Dover, 1965.

- [26] L.W. Davis. Theory of electromagnetic beams. *Phys. Rev. A*, 19:1177–1179, 1979.
- [27] S. Å. Ellingsen N. S. Aanensen and I. Brevik. Theoretical considerations of laser-induced liquid–liquid interface deformation. *Physica Scripta*, 87:055402, 2013.

5 Appendix A, Mathematica scripts.

```
ClearAll["Global`*"]
```

```
(*Script for one sided PW and Gaussian cases*)
```

```
(*Natural constants*)
```

```
 $\epsilon_0 = 8.854187817 \times 10^{-12};$ 
```

```
 $c = 299792458;$ 
```

```
(*Physical parameters*)
```

```
 $a = 2 \times 10^{-6};$  (*radius [m]*)
```

```
 $\lambda = 1.064 \times 10^{-6};$  (*wavelength [m]*)
```

```
 $w_0 = 1.5 \times 10^{-6};$  (*Laser waist: 450nm for 1064, 10 micron for 385*)
```

```
(* Parameters Oil emulsion*)
```

```
 $\gamma = 5 \times 10^{-7};$  (*surface tension, water-oil [N/m]*)
```

```
 $n_2 = 1.33;$  (*Surrounding medium is air*)
```

```
 $n_{12} = 1.41 / n_2;$  (*Relative refractive index vacuum/water*)
```

```
(*Parameters water and air
```

```
   $\gamma = 0.073;$  (*surface tension, water-oil [N/m]*)
```

```
   $n_2 = 1.33;$  (*Surrounding medium is air*)
```

```
   $n_{12} = n_2;$  (*Relative refractive index vacuum/water*)
```

```
*)
```

```
(*If setting the power directly. I use the effective power*)
```

```
 $P = 5 \times 10^{-3};$  (*Laser power*)
```

```
 $I_0 = 2 P / (\pi w_0^2);$  (*Central intensity, Gaussian beam*);
```

```
(*Total power over the droplet*)
```

```
 $P_{eff} = 0.007;$ 
```

```
(*Parameters not used in the static case*)
```

```
 $\nu = 1.01 \times 10^{-6};$  (*viscosity [m2/s]*)
```

```
 $\rho = 997;$  (*mass density difference [kg/m3]*)
```

```
(*Value of  $\alpha$  and  $\kappa$ *)
```

```
 $\alpha = N[2 \pi a n_2 / \lambda];$ 
```

```
 $\kappa = N[2 \pi w_0 n_2 / \lambda];$ 
```

```
15.707963267948962`;
```

```
11.780972450961723`;
```

```
 $I_0;$ 
```

```
1.4147106052612917`9; 1
```

```
 $a \gamma / (100 \nu^2);$ 
```

```
(*Functions and allready computed coefficients*)
```

```
(*Riccati-Bessel functions*)
```

```
 $\psi[l_, x_] := x * SphericalBesselJ[l, x];$ 
```

```
 $\psiip[l_, x_] := (1 + l) SphericalBesselJ[l, x] - x SphericalBesselJ[1 + l, x];$ 
```

```

xi[l_, x_] := x * SphericalHankelH1[1, x];
xip[l_, x_] := (1 + l) SphericalHankelH1[1, x] - x SphericalHankelH1[1 + l, x];

(*Derivative of Legendre polynomial*)
dL[l_, x_] := 
$$\frac{(-1 - l) x \text{LegendreP}[1, 1, x] + l \text{LegendreP}[1 + l, 1, x]}{-1 + x^2}$$
;

(*Loading coefficient matrices for Bessel
beams. Coefficients provided by Ellingsen.*)
TbDimI = 70;
TbDimM = 50;
TbDimN = 50;
Ilmn = Import[
  "C:\\Users\\Petter\\Desktop\\LasereBobler\\Itb70.dat"];
Mlmn = Import[
  "C:\\Users\\Petter\\Desktop\\LasereBobler\\Mtb50.dat"];
Nlmn = Import[
  "C:\\Users\\Petter\\Desktop\\LasereBobler\\Ntb50.dat"];

(*3D versions of coeffs*)
I3[l_, m_, n_] := Ilmn[[1, TbDimI (m - 1) + n]];
M3[l_, m_, n_] := Mlmn[[1, TbDimM (m - 1) + n]];
N3[l_, m_, n_] := Nlmn[[1, TbDimN (m - 1) + n]];

(*Gaussian coefficient integral that enters into A and B*)
@Integrand[l_,  $\alpha$ _,  $\kappa$ _, u_] := Sqrt[1 - u^2] LegendreP[1, 1, u]
  ( $\kappa^2 / (\kappa^2 + 2 I \alpha u)$ )^2 Exp[(- $\alpha^2 (u^2 + 1) + I \kappa^2 \alpha u$ ) / ( $\kappa^2 + 2 I \alpha u$ )];
@Integrand[l_,  $\alpha$ _,  $\kappa$ _] := NIntegrate[@Integrand[1,  $\alpha$ ,  $\kappa$ , u], {u, -1, 1}, AccuracyGoal -> 5];

(*Limit  $\kappa^2 \gg \alpha$  [plane wave limit] *)
@limit[l_,  $\alpha$ _] := 2 I^(1 + l) l (1 + l) psi[1,  $\alpha$ ] /  $\alpha^2$ ;

1

(* Using the variable beamType to determine which case is being considered.
beamType = 0 => plane wave case.
beamType = 1 => gaussian.
*)

(*Calculating the h-coefficients at time = infinity*)
hCoeffsInfty[ $\alpha$ _,  $\kappa$ _, MaxL_,  $\theta$ list_, beamType_] :=
Module[{pn, ppn, p, x, xp, cc, dd, prefac, term, h, sum, Iterm, Mterm, Nterm},
  prefac = n2 * I0 * (n12^2 - 1) / (32 c);

  (*Constants are needed in table form*)
  Print["Making tables of c and d coefficients"];
  pn = Table[psi[k, n12  $\alpha$ ], {k, 1, MaxL}];
  ppn = Table[psip[k, n12  $\alpha$ ], {k, 1, MaxL}];
  x = Table[xi[k,  $\alpha$ ], {k, 1, MaxL}];
  xp = Table[xip[k,  $\alpha$ ], {k, 1, MaxL}];
  p = Table[psi[k,  $\alpha$ ], {k, 1, MaxL}];

```

```

Which[beamType == 0,
  PhiTable = Table[Table[Limit[1, α], {1, 1, MaxL}];
  (*I0 = Peff * function(w,a)*)
  func = Pi * a ^2;
  I0 = Peff / func;
  prefac = n2 * I0 * (n12^2 - 1) / (32 c);
  ,
  beamType == 1,
  Monitor[
    PhiTable = Table[Table[Limit[1, α, κ], {1, 1, MaxL}];
    , Floor[1 * 100 / MaxL + .1] "%"];
  (*I0 = Peff * function(w,a)*)
  func = 0.5 * Pi * w0^2 * (1 - E^(-2 (a / w0)^2));
  I0 = Peff / func;
  prefac = n2 * I0 * (n12^2 - 1) / (32 c);
  ];
Print[prefac];
cc = Table[
  PhiTable[[1]] / (n12 pn[[1]] xp[[1]] - ppn[[1]] x[[1]]) / p[[1]], {1, 1, MaxL}];
dd = Table[ PhiTable[[1]] / (pn[[1]] xp[[1]] - n12 ppn[[1]] x[[1]]) / p[[1]],
  {1, 1, MaxL}];

(*CALCULATING RADIUS COEFFICIENTS*)
Print["Calculating radius perturbations"];
(*Create containers*)
σ = Table[0, {1, 1, MaxL}]; h = Table[0, {1, 1, MaxL}];
Iterm = Table[0, {1, 1, MaxL}];
Mterm = Table[0, {1, 1, MaxL}];
Nterm = Table[0, {1, 1, MaxL}];
Monitor[
  Do[
    Do[
      Do[
        Iterm[[1]] = Iterm[[1]] + cc[[m]] cc[[n]] - pn[[m]] pn[[n]] I3[1, m, n];
        Mterm[[1]] = Mterm[[1]] + α^2 (cc[[m]] cc[[n]] - ppn[[m]] ppn[[n]] +
          dd[[m]] dd[[n]] - pn[[m]] pn[[n]]) M3[1, m, n];
        Nterm[[1]] = Nterm[[1]] + I α^2 (cc[[m]] dd[[n]] - ppn[[m]] pn[[n]] -
          dd[[m]] cc[[n]] - pn[[m]] ppn[[n]]) N3[1, m, n];
        , {m, 1, MaxL}];
        , {n, 1, MaxL}];
        σ[[1]] = Iterm[[1]] + Mterm[[1]] + Nterm[[1]];
        h[[1]] = prefac * σ[[1]] * a^2 / γ / (1^2 + 1 - 2);
        , {1, 2, MaxL}];
        , Floor[1 * 100 / MaxL + .1] "%"];

Print[σ];
Print[h];

```

```

    Re[N[h]]
  ];

(*Finding a radius at time-infinity, using the h-calculator.*)
Radius[ $\alpha$ _,  $\kappa$ _, MaxL_,  $\theta$ list_, beamType_] := Module[ {h, sum},

  (*MAKING LIST OF h-Infinity COEFFICIENTS*)
  h = hCoeffsInfty[ $\alpha$ ,  $\kappa$ , MaxL,  $\theta$ list, beamType];
  SigmaTb = h / a; (*for external inspection*)

  (*Summing up the radius*)
  Print["Summing up series"];
  Monitor[
    sum = 0;
    Do[sum = sum + h[[1]] LegendreP[1, Cos[ $\theta$ list]];, {1, 2, MaxL}]
    , Floor[1 * 100 / MaxL + .1] "%"];
  Print["Done!"];
  Re[sum]
  ];

(*Calculating the time-dependence of the radius. WIP*)
TimeFunction[t_, t0_,  $\mu$ 1_,  $\mu$ 2_,  $\rho$ 1_,  $\rho$ 2_,  $\gamma$ _, a_, MaxL_] :=
  Module[{sum, gammal, omsq, mu},

  ];

(*Doubles a list by adding mirrored list -- for plotting*)
DoubleList[rList_] := Module[{target, len, dblen},
  len = Length[rList];
  dblen = 2 len - 1;
  target = Table[0, {i, 1, dblen}];
  Do[
    target[[i]] = rList[[i]];
    target[[len + i]] = rList[[len - i]];
    , {i, 1, len - 1}];
  target[[len]] = rList[[len]];
  target
  ];

(*List of theta values*)
thlength = 100;
 $\theta$ list = Table[Pi j / thlength, {j, 0, thlength}];
 $\theta$ plotlist = Table[Pi j / thlength, {j, 0, 2 thlength}];
(*Lists of radius with l up to 15,25 and 40.*)
rList15 = Radius[ $\alpha$ ,  $\kappa$ , 10,  $\theta$ list, 1]; // Timing
rList25 = Radius[ $\alpha$ ,  $\kappa$ , 25,  $\theta$ list, 1]; // Timing
rList40 = Radius[ $\alpha$ ,  $\kappa$ , 40,  $\theta$ list, 1]; // Timing

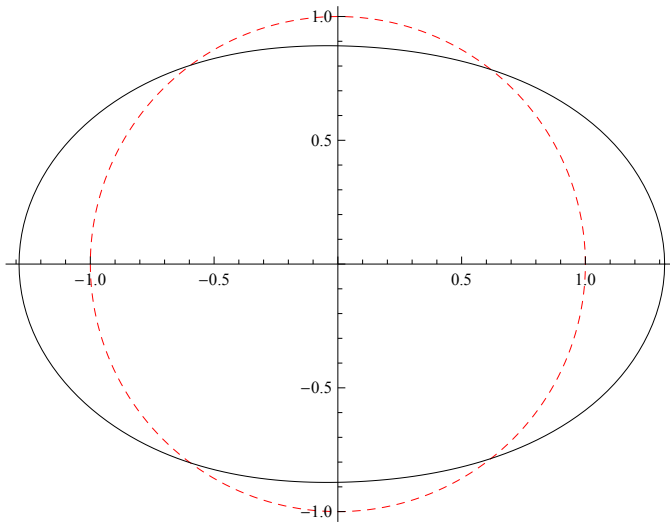
Export["C:\\Users\\Petter\\Desktop\\LasereBobler\\Oil1.5.dat", rList40, "Table"];

```

```

ListPolarPlot[{Table[{θplotlist[[i]], 1}, {i, 1, 2 thlength + 1}],
  Table[{θplotlist[[i]], 1 + DoubleList[rList25][[i]] / a}, {i, 1, 2 thlength + 1}]},
  Joined → True, PlotRange → Automatic, PlotStyle → {{Red, Dashed}, Black}]
ListPolarPlot[
  Table[{θplotlist[[i]], DoubleList[(rList40 - rList25) / (rList40)][[i]]},
    {i, 1, 2 thlength + 1}], Joined → True, PlotRange → Automatic]
ListPolarPlot[
  {Table[{θplotlist[[i]], DoubleList[rList15][[i]]}, {i, 1, 2 thlength + 1}],
    Table[{θplotlist[[i]], DoubleList[rList25][[i]]}, {i, 1, 2 thlength + 1}],
    Table[{θplotlist[[i]], DoubleList[rList40][[i]]}, {i, 1, 2 thlength + 1}] (*,
    Table[{θplotlist[[i]], DoubleList[rList50][[i]]}, {i, 1, 2 thlength + 1}] *)},
  Joined → True, PlotRange → Automatic,
  PlotStyle → {{Red, Dashed}, {Black, Dashed}, Black}]

```



```

(*Clearing the memory of old calculations and constants*)
ClearAll["Global`*"]

(*Script for the PW two sided case. l1,l2,l3 are l,l',lsigma in the text.*)

n1 = 1.41; n2 = 1.33; (*Oil emulsion parameters*)
n12 = n1 / n2;  $\gamma = 5 \cdot 10^{-7}$ ;

c = 299792458; (*speed of light [m/s]*)
 $\lambda = 1.064 \cdot 10^{-6}$ ; (*wavelength [m]*)

a =  $2 \cdot 10^{-6}$ ; (*radius [m]*)
 $\alpha = N[2 \text{ Pi } a n2 / \lambda]$ ;

Peff = 0.028;
maxL = 17;

coeffs = Import["PwtsCoeffs2-17.wdx"];
coeffsL = coeffs[[1]];
coeffI = coeffs[[2]];
coeffM = coeffs[[3]];
coeffN = coeffs[[4]];

If[maxL > coeffsL,
  Print["Not enough coefficients computed! Making due with a maxL of: ",
    coeffsL]; maxL = coeffsL;];
Print["Alpha: ",  $\alpha$ , " Max L: ", maxL];

(*Tables for the spherical functions*)
psi[l_, x_] := x * SphericalBesselJ[l, x];
psip[l_, x_] := (1 + l) SphericalBesselJ[l, x] - x SphericalBesselJ[1 + l, x];
xi[l_, x_] := x * SphericalHankelH1[l, x];
xip[l_, x_] := (1 + l) SphericalHankelH1[l, x] - x SphericalHankelH1[1 + l, x];
pn = Table[psi[k, n12  $\alpha$ ], {k, 1, maxL}];
ppn = Table[psip[k, n12  $\alpha$ ], {k, 1, maxL}];
x = Table[xi[k,  $\alpha$ ], {k, 1, maxL}];
xp = Table[xip[k,  $\alpha$ ], {k, 1, maxL}];
p = Table[psi[k,  $\alpha$ ], {k, 1, maxL}];

(*Calculating the A coefficients*)
aL = Table[0, {1, 1, maxL}];

Do[
  integrandA1[u_] := Exp[i *  $\alpha$  * u] * LegendreP[1, 1, u] * Sqrt[(1 - u^2)];
  aL[[1]] =  $\frac{1}{1(1+1) * p[[1]]} \text{Sqrt}\left[(2 \cdot 1 + 1) * \frac{\text{Pi}}{1(1+1)}\right] *
    NIntegrate[integrandA1[u], {u, -1, 1}, AccuracyGoal \to 5];$ 
```

```

, {1, 1, maxL}]

(*Core-function that runs to calculate sigma for all l1,l2.*)
sigmaForL[l1_, l2_, l3_] := Module[{sigma, sigmaLM},

  utListe = {0, 0, 0};

  a1 = aL[[l1]];
  b1 = -I * n2 * a1;
  a2 = aL[[l2]];
  b2 = -I * n2 * a2;

  (* c,d as per Barton*)
  c1s = I * a1 / (n12 * n12 * pn[[l1]] * xp[[l1]] - n12 * ppn[[l1]] * x[[l1]]);
  d1s = I * b1 / (pn[[l1]] * xp[[l1]] - n12 * ppn[[l1]] * x[[l1]]);
  (*Remember that the second field is conjugated*)
  c2s =
  N[Conjugate [I * a2 / (n12 * n12 * pn[[l2]] * xp[[l2]] - n12 * ppn[[l2]] * x[[l2]])]];
  d2s = Conjugate [I * b2 / (pn[[l2]] * xp[[l2]] - n12 * ppn[[l2]] * x[[l2]])]];

  place = (l1 - 1) * coeffsL * coeffsL + (l2 - 1) * coeffsL + l3;

  Do[
  Switch[i, (*Same as in the parameter generating code*)
  1, m1 = 1; m2 = 1; utPlace = 2;,
  2, m1 = 1; m2 = -1; utPlace = 3;,
  3, m1 = -1; m2 = 1; utPlace = 1;,
  4, m1 = -1; m2 = -1; utPlace = 2;];
  (*Handling the sign flips in A. Quick and Dirty*)
  If[Mod[l1, 2] == 0 && (m1 == -1), c1 = -c1s; d1 = -d1s;, c1 = c1s; d1 = d1s;];
  If[Mod[l2, 2] == 0 && (m2 == -1), c2 = -c2s; d2 = -d2s;, c2 = c2s; d2 = d2s;];

  factorToUtliste =
  (coeffI[[place]][[i]] l1 (l1 + 1) l2 (l2 + 1) c1 * c2 * pn[[l1]] * pn[[l2]] +
  coeffM[[place]][[i]]  $\alpha * \alpha$  (n12 * n12 * c1 * c2 * ppn[[l1]] * ppn[[l2]] +
   $\frac{1}{n2 * n2}$  d1 * d2 * pn[[l1]] * pn[[l2]]) +
  coeffN[[place]][[i]]  $\alpha * \alpha$  (d1 * c2 * pn[[l1]] ppn[[l2]] +
  c1 * d2 * ppn[[l1]] * pn[[l2]]));

  utListe[[utPlace]] = utListe[[utPlace]] + factorToUtliste;

, {i, 1, 4}];

```

```

Return[utListe]
];

sigmaFinal = Table[{0, 0, 0}, {1, 1, maxL}];

Do[
Do[
Do[
sigmaSpam = sigmaForL[l1, l2, l3];
sigmaFinal[[l3]] = sigmaSpam;
, {l3, 2, maxL}]
, {l2, 2, maxL}]
, {l1, 2, maxL}]

r[the_, phi_] = 1; (*r=r/a*)

Do[
spam = sigmaFinal[[1]];
prefacR =  $\frac{\text{Peff}}{\gamma (1 * 1 + 1 - 2) a^8 \text{Pi} c} \frac{n2}{(n12 n12 - 1)}$ ;
(*Not the extra a to normalize a = r/a*)

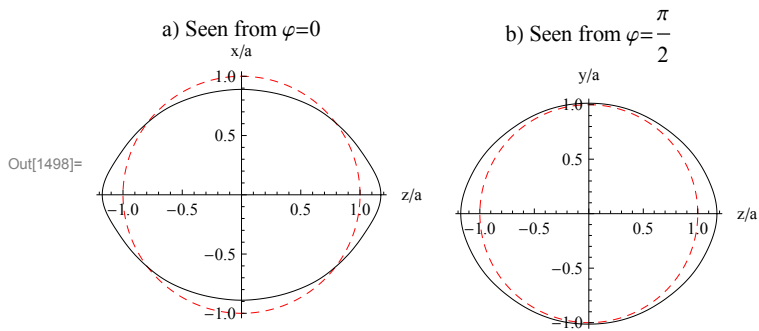
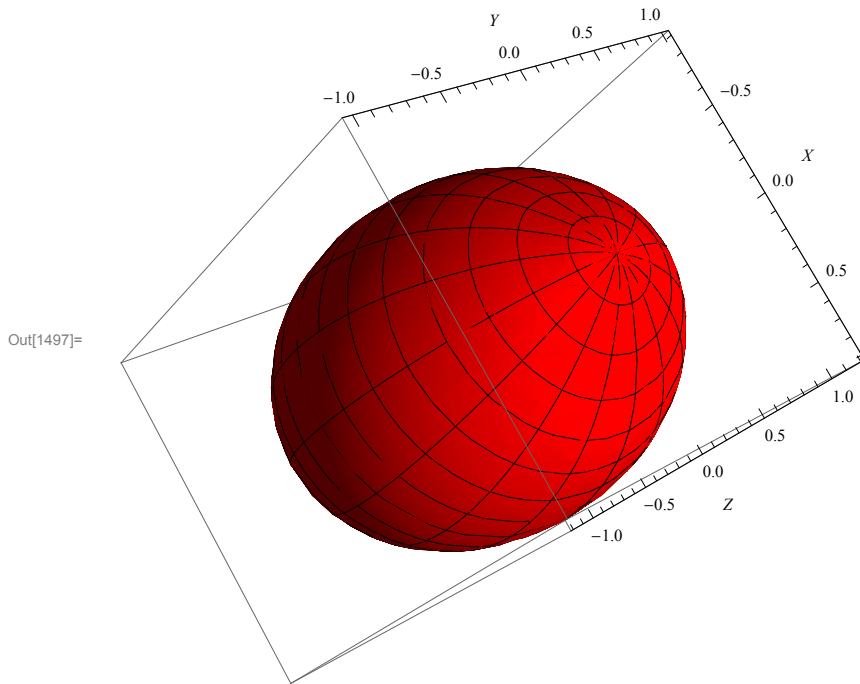
toAdd[the_, phi_] := spam[[1]] * Exp[-I * 2 * phi] * LegendreP[1, -2, Cos[the]] +
spam[[2]] * LegendreP[1, 0, Cos[the]] +
spam[[3]] * Exp[I * 2 * phi] * LegendreP[1, 2, Cos[the]];

r[the_, phi_] = r[the, phi] + prefacR * Re[toAdd[the, phi]];
, {1, 2, Length[sigmaFinal]}];

(*Plotting. The clutter is simply generating the specific looks of the plots.*)
SphericalPlot3D[Re[r[the, phi]], {the, 0, Pi},
{phi, 0, 2 Pi}, AxesLabel -> {X, Y, Z}, PlotStyle -> {Red}]
GraphicsGrid[
{
{
PolarPlot[{1, Re[r[theta, 0]]}, {theta, 0, 2 Pi}, PlotStyle -> {{Red, Dashed}, Black},
AxesLabel -> {"z/a", "x/a"}, PlotLabel -> "a) Seen from phi=0"},
PolarPlot[{1, Re[r[theta, Pi/2]]}, {theta, 0, 2 Pi}, PlotStyle -> {{Red, Dashed}, Black},
AxesLabel -> {"z/a", "y/a"}, PlotLabel -> "b) Seen from phi= $\frac{\pi}{2}$ "}]}]}

```

Alpha: 15.708 Max L: 17



In[1499]= **Export["OilEmulsion.png", %1498, "PNG"]**

Out[1499]= OilEmulsion.png

```

ClearAll["Global`*"]
(*Calculating the coefficients needed
for the new cases considered. m1,m2 = +-1.*)

nextMaxL[Coeffs_] :=
Module[{}, (*Calculates the coefficients for maxL+1 from coeffs for maxL*)

(*Defining variables and paramters*)
Lold = Coeffs[[1]];
L = Lold + 1;
termsNew = L * L * L;

old1 = Coeffs[[2]];
old2 = Coeffs[[3]];
old3 = Coeffs[[4]];

new1 = Table[{0, 0, 0, 0}, {i, 1, termsNew}];
new2 = Table[{0, 0, 0, 0}, {i, 1, termsNew}];
new3 = Table[{0, 0, 0, 0}, {i, 1, termsNew}];

Do[
  Do[
    Do[

(*1D list → 3d list*)
place = (l1 - 1) * L * L + (l2 - 1) * L + l3;

If[(l1 ≤ Lold) && (l2 ≤ Lold) && (l3 ≤ Lold),
placeOld = (l1 - 1) * Lold * Lold + (l2 - 1) * Lold + l3;
new1[[place]] = old1[[placeOld]];
new2[[place]] = old2[[placeOld]];
new3[[place]] = old3[[placeOld]];
,

integrand1[u_, m1_, m2_, m3_] :=
LegendreP[l1, m1, u] LegendreP[l2, m2, u] LegendreP[l3, m3, u];
integrand2[u_, m1_, m2_, m3_] := (1 - u^2) *
D[LegendreP[l1, m1, u] LegendreP[l2, m2, u], u] LegendreP[l3, m3, u] +
m1 * m2
(1 - u^2) * LegendreP[l1, m1, u] LegendreP[l2, m2, u]
LegendreP[l3, m3, u];
integrand3[u_, m1_, m2_, m3_] := m1 * LegendreP[l1, m1, u]
D[LegendreP[l2, m2, u], u] LegendreP[l3, m3, u] +
m2 * D[LegendreP[l1, m1, u], u] LegendreP[l2, m2, u] LegendreP[l3, m3, u];

```

```

Do[
  Switch[i,
    1, m1 = 1; m2 = 1;,
    2, m1 = 1; m2 = -1;,
    3, m1 = -1; m2 = 1;,
    4, m1 = -1; m2 = -1;];

  m3 = m1 - m2;
  If[Abs[l3] ≥ Abs[m3],
    prefacK = Sqrt[(2 l1 + 1)  $\frac{((11 - m1)!)^2}{4 \text{Pi} ((11 + m1)!)}$ ]
      Sqrt[(2 l2 + 1)  $\frac{((12 - m2)!)^2}{4 \text{Pi} ((12 - m2)!)}$ ] (2 l3 + 1)  $\frac{((13 - m3)!)^2}{2 ((13 + m3)!)}$ ;

    new1[[place]][[i]] = prefacK *
      NIntegrate[integrand1[u, m1, m2, m3], {u, -1, 1}, AccuracyGoal → 5];
    new2[[place]][[i]] = prefacK * NIntegrate[integrand2[u, m1, m2, m3],
      {u, -1, 1}, AccuracyGoal → 5];
    new3[[place]][[i]] = prefacK * NIntegrate[integrand3[u, m1, m2, m3],
      {u, -1, 1}, AccuracyGoal → 5];

  ]
  , {i, 1, 4}
]

, {l3, 1, L}];
, {l2, 1, L}];
, {l1, 1, L}];

finalCoeff = {L, new1, new2, new3};

Return[finalCoeff];
]

A = Import["PwtsCoeffs2-15.wdx"];
B = Nest[nextMaxL, A, 1];
Export["PwtsCoeffs2-17.wdx", B];
Beep[];
(*A = Import["PwtsCoeffs30.wdx"];
Print[A[[1]]];
B = nextMaxL[A];
Beep[];
Export["PwtsCoeffs31.wdx", B];*)

```

```
Print[B[[1]]];
```

17